ANKARA YILDIRIM BEYAZIT UNIVERSITY GRADUATE SCHOOL OF NATURAL AND APPLIED SCIENCES

MICROFLUIDIC INTEGRATION ONTO GOLD MICROELECTRODE AND ITS EFFECT ON ELECTROCHEMISTRY

M.Sc. Thesis by

Zahraa Ali

Department of Material Engineering

September 2021

ANKARA

MICROFLUIDIC INTEGRATION ONTO GOLD MICROELECTRODE AND ITS EFFECT ON ELECTROCHEMISTRY

A Thesis Submitted to

The Graduate School of Natural and Applied Sciences of

Ankara Yıldırım Beyazıt University

In Partial Fulfillment of the Requirements for the Degree of Master of Science in Material Engineering, Department of Material Engineering

by

Zahraa Ali

September 2021

ANKARA

M. Sc. THESIS EXAMINATION RESULT FORM

We have read the thesis entitled **"MICROFLUIDIC INTEGRATION ONTO GOLD MICROELECTRODE AND ITS EFFECT ON ELECTROCHEMISTRY"** completed by **ZAHRAA ALI** under the supervision of **ASSIST. PROF. DR. FATMA DOGAN GUZEL** and we certify that in our opinion it is fully adequate, in scope and quality, as a thesis for the degree of Master of Science.

Assist. Prof. Dr. Fatma DOĞAN GÜZEL

Supervisor

Assist. Prof. Dr. Begüm ÜNVEROĞLU

Jury Member

Assist. Prof. Dr.Aligül BÜYÜKAKSOY

Jury Member

Prof. Dr. Prof. Dr. Sadettin ORHAN

Director

Graduate School of Natural and Applied Sciences

ETHICAL DECLARATION

I hereby declare that, in this thesis which has been prepared in accordance with the Thesis Writing Manual of Graduate School of Natural and Applied Sciences,

- All data, information, and documents are obtained in the framework of academic and ethical rules,
- All information, documents, and assessments are presented in accordance with scientific ethics and morals,
- All the materials that have been utilized are fully cited and referenced,
- No change has been made on the utilized materials,
- All the works presented are original, and in any contrary case of the above statements, I accept to renounce all my legal rights.

Date: 22.09.2021 **Signature:**

Zahraa Ali

ACKNOWLEDGMENTS

I would like to thank my supervisor Assist. Prof. Dr. Fatma Dogan Guzel for her great support and patience throughout my studies. She always shared her vast knowledge, recommendations, and experiences with me at every step of my thesis. Her help, motivation, and guidance continued with me on the last day of research. I am grateful to her for standing by my side every time I feel frightened and frustrated.

I would also like to thank Dr. Ahmet Uçar for his extensive knowledge and assistance by providing information and advice.

In addition, I would also like to thank the members of the Biomedical Engineering Lab group for their support and for facilitating some of the difficulties I encountered during my research career (Dr. Hamed Ghorbanpoor, Dr. Araz Norouz Dizaj, Yasin Ozturk, Iremnur Akçakoca and, Jaspreet Kaur).

I would like to extend my gratitude to Prof. Abdullah Yıldız and his laboratory team for allowing me to perform the AFM characterization in his Energy System Laboratory at AYBU. I also would like to thank Mr. Abdullah Atılgan for his assistance to make AFM and SEM characterization.

This thesis would not have been possible unless working at National Nanotechnology Research Center UNAM, Bilkent University.

I would like to express my very deep appreciation to the best parents in the world, my mum and dad for their love, constant encouragement, and trust, and I do not forget the role of encouraging the best brothers in the world (My Brothers).

The research in this dissertation was supported by TUBITAK under Grant No: 217S793.

2021, 22 September **Zahraa Ali**

MICROFLUIDIC INTEGRATION ONTO GOLD MICROELECTRODE AND ITS EFFECT ON ELECTROCHEMISTRY

ABSTRACT

Integrated microfluidic devices are used in many medical, biological, and other applications due to their characteristics such as small size, sensitivity, reduced amount of needed analyte, ease of use, and accuracy of results. However, it has been noted the results depend on many variables, the most important of which is the electroactive area of the working electrode. In this study, Square Wave Voltammetry (SWV), Cyclic Voltammetry (CV), and Differential Pulse Voltammetry (DPV) have been used for examining four devices with working electrodes with varying electroactive areas altered by changing the size of the integrated channels (50, 100, 250, and 500 µm). The dimensions of the channels are directly related to the surface area of the working electrode. This study aimed to comprehend the changes in electrochemical responses such as macroelectrode-to-microelectrode conversion, limiting currents, the effect of scan rate. Also, Scanning Electron Microscopy (SEM), and Atomic Force Microscopy(AFM) measurements were performed to analyze the nature of the electrode surface in terms of roughness and microstructure. The performance of the electrodes was determined by estimating the working areas for each electrode and conducting electrochemical and microscopic examinations for them. It was observed that when the effective area of the electrode becomes larger, the performance of the electrodes becomes better, and gives more accurate and definite results.

Keywords: Cyclic voltammetry (CV), lab-on-chip, microelectrode, macroelectrode.

MİKROELEKTROTLARA MİKRO AKIŞKAN ENTEGRASYONU VE ELEKTROKİMYA ÜZERINDEKI ETKİSİ

ÖZ

Entegre mikroakışkan cihazlar, küçük boyut, hassasiyet, azaltılmış gerekli analit miktarı, kullanım kolaylığı ve sonuçların doğruluğu gibi özelliklerinden dolayı birçok tıbbi, biyolojik ve diğer uygulamalarda kullanılmaktadır. Bununla birlikte, sonuçların, en önemlisi çalışma elektrotunun elektroaktif alanı olan birçok değişkene bağlı olduğu not edilmiştir. Bu çalışmada Kare Dalga Voltametrisi (SWV), Döngüsel Voltametri (CV) ve Diferansiyel Darbe Voltametrisi (DPV), entegre kanalların boyutu değiştirilerek değişen elektroaktif alanlara sahip dört cihazı incelemek için kullanılmıştır (50, 100, 250, ve 500 um). Kanalların boyutları doğrudan çalışma elektrotunun yüzey alanı ile ilgilidir. Bu çalışma, makroelektrot-mikroelektrot dönüşümü, sınırlayıcı akımlar, tarama hızının etkisi gibi elektrokimyasal tepkilerdeki değişiklikleri kavramayı amaçlamıştır. Ayrıca, elektrot yüzeyinin yapısını pürüzlülük ve mikro yapı açısından analiz etmek için Taramalı Elektron Mikroskobu (SEM) ve Atomik Kuvvet Mikroskobu (AFM) ölçümleri yapılmıştır. Elektrotların performansı, her elektrot için çalışma alanları tahmin edilerek ve elektrokimyasal ve mikroskobik incelemeler yapılarak belirlenmiştir. Elektrotun etkin alanı büyüdükçe elektrotların performansının daha iyi olduğu, daha doğru ve kesin sonuçlar verdiği gözlemlenmiştir.

Anahtar Kelimeler: Döngüsel voltametri (CV), çipte-Lab, mikroelektrot, makroelektrot.

CONTENTS

NOMENCLATURE

CV	Cyclic Voltammetry
DPV	Differential Pulse Voltammetry
SWV	Square Wave Voltammetry
Au	Gold
Cr	Chromium
V	Voltage
I	Current
SPEs	Screen Printed Electrodes
H_2SO_4	Sulfuric acid
DI	Deionized
AFM	Atomic Force Microscopy
PDMS	Polydimethylsiloxane

LIST OF TABLES

LEST OF FIGURES

CHAPTER 1

INTRODUCTION

Electrochemistry is the study of the relationship between chemical reactions and electrical changes (current and voltage). It has great importance in the great advances in technology that helped in many fields such as pollution control, organic and inorganic synthesis, sensing, and energy applications as shown in Figure 1.1. Since the early sixteenth and seventeenth centuries, electrochemistry underwent many developments that began with theories of magnets and extended to complex theories involving the transfer and conductivity of electrical charges [1]. In the 1950s, the development of electrochemistry was so great that the principles of chemicals were applied to describe the electrochemical interaction and electrode interactions related to the current-voltage control of the working electrode [2]. The introduction of electrochemical equipment progressed the development of the use of potentials of voltage and current in electrochemical experiments, that happened through a technique called "stationary electrode polarography" represented by searching the current by repeatedly scanning a fixed triangular wave with different scan rates and the possibility of applying the current in the opposite direction, which used to allow the researcher to know a lot of information related to the experiment [3-4]. The examination of "cyclic voltammetry" and the information it provided has aroused vast interest in the most complex electrochemical reactions [5]. Electrochemical cells were one of those developments in the principle of which they work by depositing dissolved ions on the cell's electrodes. The use of electrodes was an effective performance for more reliable measurement and control of the current passing through the cell to obtain redox potentials using voltametric measurements [6].

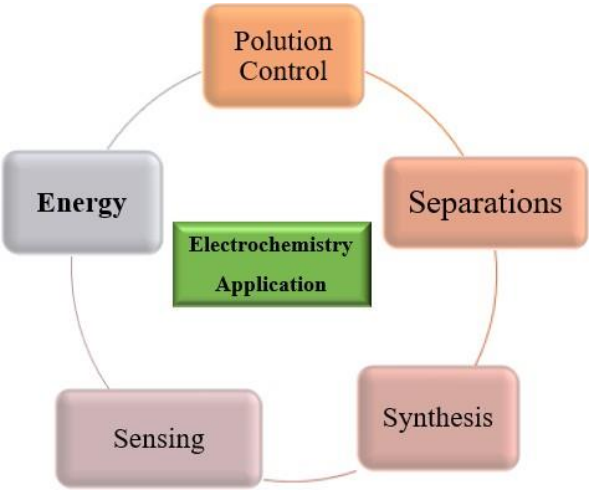

Figure 1.1 Electrochemistry application.

1.1 Overview of Electrodes

An electrode is a conductive object that can be described as the point of current entering or leaving a cell. The anode is the electrode at which electrons leave the cell, and oxidation occurs at it and is known as the anode. The electrons enter the cell, where the process of reduction occurs and at this point, the electrode is known as the cathode [7-8]. The type of electrode is determined depending on the direction of the electron flow. The surface of the electrode can be modified with other stimuli, films, or metals to make the electrode more sensitive and/or more selective to the analyzer [9]. Electrodes in general have wide applications in different fields as shown in Figure 1.2. The broadest and first application was around the 1980s, by the creation of electrical signals resulting from neurophysiological mechanisms [10-11]. Due to its small size, which reaches the nano-level, it does not inflict any damage on the cell to be examined. Metal electrodes are used to measure periodic voltage or electric current [12]. The electrodes have a long history of experimental study in electrochemical measurements because they provide unparalleled ultra-accurate results compared with other methods [12].

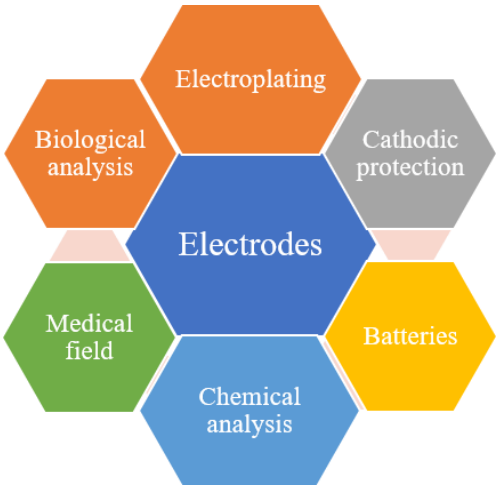

Figure 1.2 Electrodes using areas.

1.2 Electrode system in an electrochemical cell

Set-up of electrode system can be two types: two electrode system and three electrode system.

1.3 Three electrode system

The purpose of using three electrodes in a cell is to study the behavior of the analyte in detail and the electrochemical behavior of materials not like a bipolar cell, which only shows us the current flow between the two electrodes. In the three-electrode system, there are three electrodes: working electrode, reference electrode, and counter electrode [13].

1.4 Working Electrode

The working electrode is an essential component in the process in which the most important cell interactions, and electron transfer processes such as electron gain or loss represented by oxidation and reduction processes, or both, direct the electrochemical reaction path according to its properties: materials, adsorbent surface, etc. [14-15]. The choice of materials for the working electrode is very important for the success of the experiment, but this requires consideration of several factors that will be mentioned later [16].

1.5 Reference Electrode

The reference electrode is the electrode that has a stable and known potential against another potential of the cell. Reference electrodes are used to set the relative potential of a solution in an electrochemical cell [17]. To obtain a well-functioning reference electrode, its components must be kept stable and not significantly altered during the electrochemical measurement process. The static potential of the reference electrode regulates the potential of the working electrode and measures the voltage without current passing through it. The ideal reference electrode should have zero impedance [18-19].

1.6 Counter (auxiliary) Electrode

The counter electrode is one of the components of a three-electrode electrochemical cell, which completes the electrical circuit and provides the current required for the working electrode [20]. The counter electrode has a surface area larger than that of the working electrode to ensure that current restrictions do not appear. [21]. In cell reactions, the potentials of the counter electrode are not measured, but they are adjusted to balance the reaction occurring in the working electrode, and it is together with the working electrode as it serves to provide a circuit in which the current is applied and measured. The presence of the counter electrode helps to measure the potential of the working electrode against the known potential of the reference electrode without compromising its stability bypassing current over it [22].

1.7 Types of Electrodes

The production of the electrodes is also important because it may affect the effectiveness of the measurement and the process, as there are many electrodes made of different materials and of different sizes. In this section, the choice of materials and their size will be examined, respectively.

1.8 Material types of Electrodes

The choice of electrode materials requires consideration of several factors including electrical conductivity, biocompatibility, and high corrosion resistance [23] ,and consistent oxidation and reduction behavior with the analyte and electron transport

processes in a fast and reproducible manner without electrode contamination, and the ease of forming the metal into different shapes suitable for practical purposes as well as its toxicity. The most common electrode materials are platinum, gold, carbon, and mercury. Among these materials, platinum may be the best due to its high electrochemical inertness. Regardless of its high cost, it has another disadvantage, which is that even with the presence of a small amount of water in the solution, it works to form hydrogen gas more than the hydrogen reduction method, which in turn, blocks any useful analytical signals [24]. As for carbon electrodes, their disadvantage is that they are highly susceptible to mechanical damage in addition to their cost and difficulty in manufacturing [25]. Regarding mercury, despite its width as a potential window for the cathode, its disadvantage is that it is easy to oxidize when the anode window is displayed, the dropping mercury electrode (DME) forms droplets that frequently fall off during the potential scan. which prompts it to be replaced in every new experiment. [26]. The specifications of gold compared to other metals specifications were the best in terms of oxidation, reduction, toxicity, corrosion, and its use for a long term without changing the electrode properties [27]. In Table 1-1, the commonly used materials will be compared in terms of advantages and drawbacks.

Table 1-1 Advantages and limitations of electrode materials.

material	Advantages	Drawbacks
Platinum (Pt)	Good electrochemical inertness and ease of manufacture in many forms.	Hydrogen ion reduction Expensive
Gold (Au)	larger range of cathodic potential	Expensive
Carbon (C)	Good range of cathodic potential	Highly susceptible to mechanical damage
Mercury (Hg)	Excellent range of cathodic potential	Easy to oxidize when the anode window is displayed

1.9 Characterization of Size of Electrodes

The size is a very important factor in determining the response of the electrodes. The difference between macro-, micro-, and nanoelectrodes lies in the size, where the size of macroelectrode is above 100µm, while the size of microelectrodes reaches to micrometer scale (a few tens of micrometers or less), and nanoelectrodes reach below 100 nm. Micro and nanoelectrodes were commonly used as probes in chemical analysis due to their ability to reach inaccessible places and their ability to examine small numbers of electrically active particles, [28-30]. The use of microelectrodes helps to improve mass transfer, as and thus higher current densities[1] [31]. Microelectrodes also have other benefits like the ability to perform electrochemical tests in highly denatured solutions improving the signal-to-noise ratio, giving the possibility of expanded use of potentiometric techniques and chronometers in analytical chemistry. The difference in the size of the electrode, whether it is macro or micro, affects several related matters to the experiment, such as the mass transfer or the rate of diffusion, whereas the diffusion field develops with the development of the electrode size, and this means that the solid angle developed by the diffusion layer above the electrode surface increases dramatically with the increase in the electrode surface size, and this enhances the occurrence of linear diffusion. The diffusion turns from linear to hemispherical (radiative), as shown in Figure 1.3. This is much better than linear diffusion, in terms of the importance of the current enhancement and propagation. Thus, it gives more sensitive and accurate results, as it becomes easier due to the steady-state it provides [32-34], In one the literature, it has been assumed that the diffusion on the electrode surface is flat at the middle, but at the edges of the electrode it is uneven, as the size of the electrode decreases, the diffusion becomes more dominant, the shape of the electrode becomes less important when the rate of oxidation and reduction is on the electrode for a period during which the longest dimension of the electrode is much less compared to the diameter [35].

[1]Current density is the magnitude of charge per unit time flowing through a unit area of a chosen cross-section

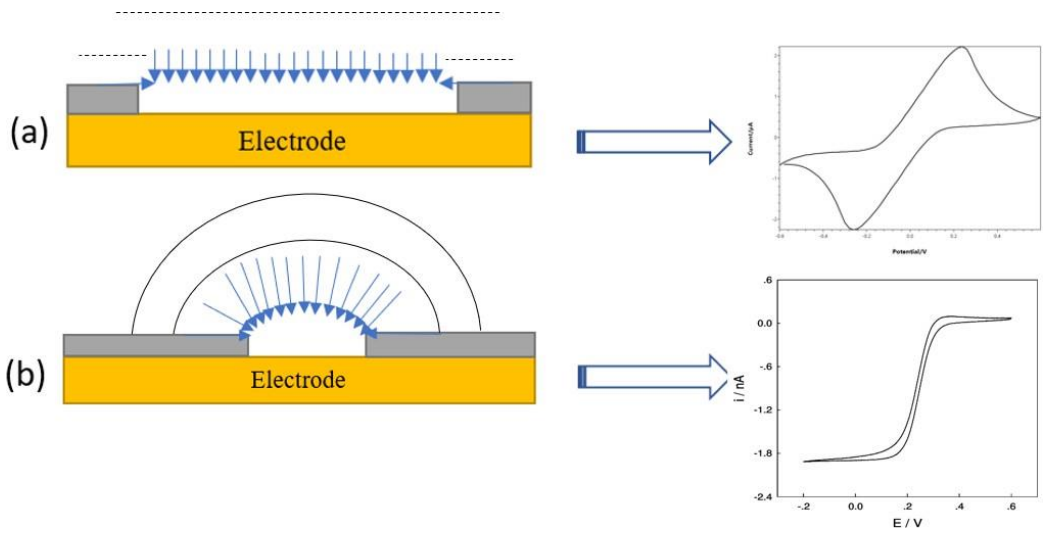

Figure 1.3 Diffusion to the electrode, the arrows represent the diffusion of the substance on the electrode a) Macro electrode, where planar diffusion dominates. b) Microelectrode is progressively smaller as planar propagation is no longer dominant.

Faster reactions can be achieved by raising the mass transfer rate [36]. Electrode interactions include electron transfer processes on the electrode and solutions. Since the electron transfer rate is affected by the electrode potential through an exponential relationship, the current also increases dramatically [37]. Mass transfer can be achieved whether the electrode is a macroelectrode or microelectrode to nanoelectrode, and the smaller the electrode size, the greater the possibilities of achieving higher current densities. [38]. Mass transport can be represented by three types that affect the electrochemical reaction as shown in Figure 1.4, namely:

- Diffusion occurs in solutions that have unequal concentrations as the entropy standardizes these concentrations by moving the mass from areas of high concentration to areas of low concentration [39].

- Convection is a single or multi-phase flow that occurs due to the heterogeneity of the properties of the materials and the different gradients of density in which the movement on the surface of the electrode is by a physical movement and the driving force of this movement is a mechanical force resulting from magnetic or gravitational forces resulting from the flow or flow of the solution [39].

- Migration is the movement of charged particles because of being subjected to an electrostatic force [40].

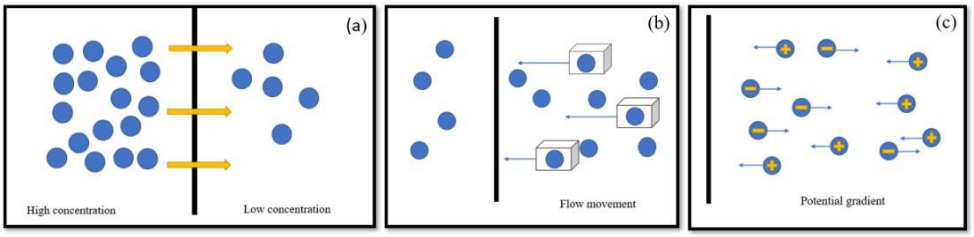

Figure 1.4 Mass transformation in microelectrodes :a) Diffusion, b) Convection and c) Migration.

1.10 Fabrication of Electrodes

The method of manufacturing the electrode and the properties of the materials greatly affect the quality of the electrode. The common process for manufacturing electrodes is to deposit the metal, either by gas or electric methods, as thick films or thin films [41]. In general, the electrode can be manufactured from several layers to obtain the optimum electrode. The first layer is the substrate or the base layer, and it is often made of glass, which is preferred because of its consumption of less energy and its very low conductivity [42] ,the second layer is the deposit of metal such as chromium (Cr) or titanium (Ti) , which is used to enhance the adhesion of gold to the glass substrate.

1.11 Type of Electrochemical techniques

Electrochemical techniques have been used in many analytical fields that examine various phenomena such as spectroscopy [43] Electrochemical techniques are widely applied to describe the oxidation and reduction reactions that occur in the electrochemical cell. They generally relay on the electrochemical cell response through the application of electrical input by the electrodes of the cell immersed in the electrolyte and capability of electron transfer [44]. Electrochemical techniques are divided into three types: voltametric, potentiometric, and impedimetric [45]. In a voltametric technique , the voltage is applied while the current is measured, and it is divided according to the input capabilities. If a constant voltage is applied and then the current is measured, this is called Amperometry. If increasing linear potentials are

provided, this is called Linear Sweep Voltammetry, triangular wave potentials are introduced, it is called Cyclic Voltammetry (CV), and it is called Chronoamperometry for square wave potentials and so on. In Potentiometric measurements, a constant current is applied, and potential is measured while in Impedimetric method alternating voltage is applied and impedance is measured. It was reported that potentiometric approach is one of the best techniques used to understand the electron transfer mechanism [46]. However, several factors such as application and/or electrochemical approach may affect the choice. In general, all these techniques provide exclusive information, including the reaction mechanism, the chemical state of the reactants in the solution, and the kinetics of the electrodes. Due to the different operating electrode types and parameters available in electrochemical experiments, there are several techniques that are used in electrochemical principles. Some of them will be examined in detail in the following sections:

1.12 Cyclic Voltammetry (CV)

Cyclic voltammetry is one of the most used techniques in electrolysis. It can study the electrochemical properties of analysis in a solution or a molecule that is absorbed on an electrode and, also works to measure the current that develops in the electrochemical cell and is done by cycling the working electrode voltage and measuring the resulting current [47]. Simply, the potential of the working electrode is applied in a linear manner with time, and when the potential reaches a certain limit E2, the potential of the working electrode is applied in reverse to return to the potential starting point E1, which is returned with a constant scanning rate υ, as shown in Figure 1.5.

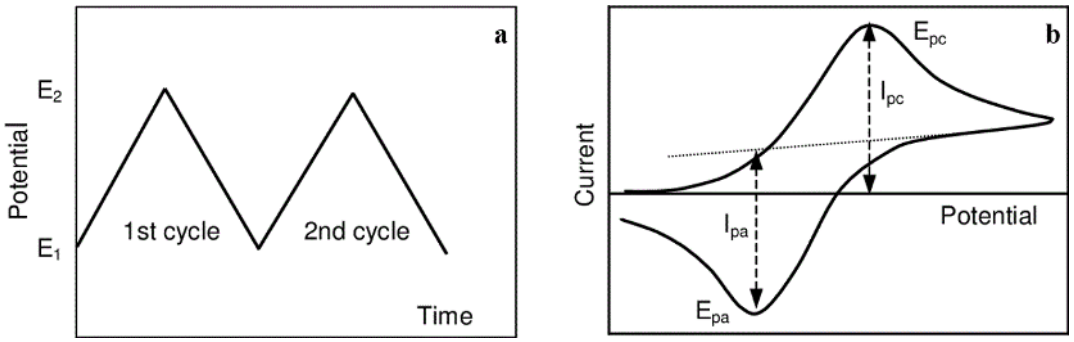

Figure 1.5 Cyclic Voltammogram diagram. (a) Demonstrates a triangular potential waveform, (b) The cyclic voltammogram diagram shows redox reactions as Ipc, the cathodic peak current; Ipa, anodic peak current; Epc, the cathodic peak potential; Epa, the anodic peak [47].

These cycles can be applied as many times as needed until the shape stays unchanged [48]. During the first anterior examination, an increased reduction potential is applied. Therefore, the cathodic current will increase, at least in the beginning. The presence of a reducible analyte in the system, and after reaching the reducing potential. The cathodic current begins to decrease with the depletion of the concentration of the reducible analyte, and the re-oxidation of the reducible analyte begins upon reverse scanning. In the cyclic voltammetry, the obtained current does not depend only on the concentration and electrical properties of diffusion, but also on the scan rate, which represents the rate of change of potentials with time, is described by the equation below [49].

$$\square_{\square} = 0.4463\square\square\square\square \left(\frac{\square\square\square\square}{\square\square}\right)^{\frac{1}{2}} \quad \textbf{(1.1)}$$

Or if the solution is at 25 °C

$$\square_{\square} = 2.69 \times 10^{5} \square^{\frac{3}{2}} \square^{\frac{1}{2}} \square^{\frac{1}{2}} \quad \textbf{(1.2)}$$

Where i_p is maximum current in amperes, n is number of electrons transferred in the redox reaction, A is electrode area in cm^2, F is Faraday Constant in C mol^{-1}, D is diffusion coefficient in cm^2/s, C is concentration in mol/cm^3, ν is scan rate in V/s, R is Gas constant in J $K^{-1}mol^{-1}$ and, T = temperature in K.

Since I_p is the current or passage of electrons per unit time, that the current can increase when the rates of scanning potentials are faster. The current is restricted by the diffusion on the surface of the electrode and that the rate of diffusion is affected by the difference in the concentration and speed of diffusion on the surface of the electrode, this happened by changing the potential of the electrochemical cell This can be represented by the Nernst equation [50].

$$E_{cell} = E^0 - \frac{RT}{nF} \ln Q \quad \textbf{(1.3)}$$

Where, E^0 = cell potential under the standard conditions, E_{cell} is cell's cell potential, T is temperature, R is the universal gas constant, n is number of electrons transferred during the redox reaction, Q is reaction quotient and F is faraday constant. Therefore, it is clear to say that the concentration is greater near the electrode due to the increase in the speed of the voltage scanning rate, which results in a higher current.

1.13 Square Wave Voltammetry (SWV)

It is one of the electrochemical techniques used in the study of the thermodynamics of chemical, mechanical, and kinetic reactions and in conducting quantitative chemical analysis through a united square wave and ladder potential applied to an immutable electrode. The current of the working electrode is measured, while the potentials of the working and reference electrode are in forward and backward movement at a fixed frequency. In this examination, the test is taken twice, once for the forward pulse potential and the second time for the reverse pulse potential. SWV is used in potentiometric programs to draw a differential current wave that is derived by deducting the reverse current waveform from the forward current waveform and drawing the differential curve against the applied potentials where the peaks refer to the oxidation and reduction processes. The peaks vary with different concentrations, as shown in Figure 1.6 [51]. The frequency used in SWV testing ranges from 1Hz to

125 Hz, which means that square wave measurement is usually much faster than other pulse voltammetry experiments.

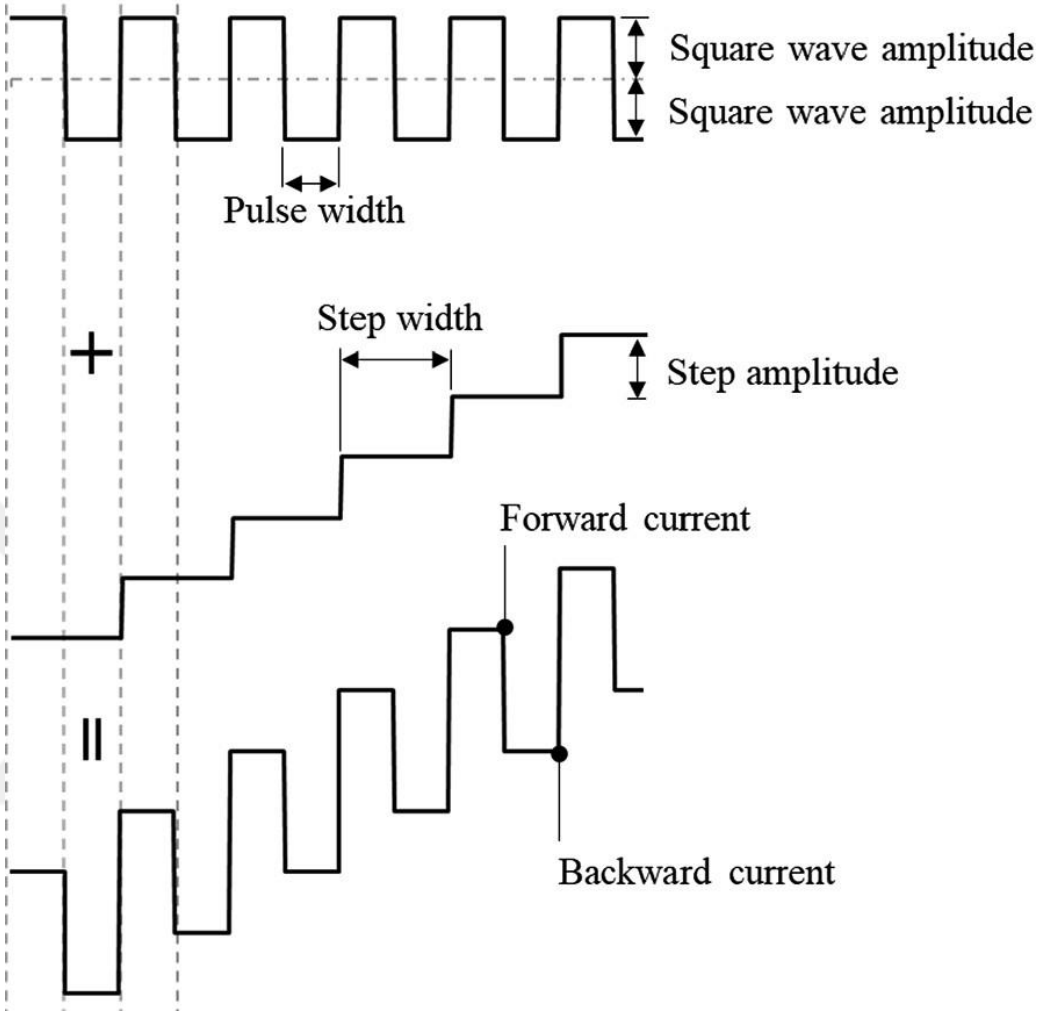

Figure 1.6 Schematic diagram of scanning waveform of square wave voltammetry, which is the sum of a symmetrical square wave and a ladder wave of the same frequency and phase. Adapted from [51].

1.14 Differential Pulse Voltammetry (DPV)

Differential pulse voltammetry (DPV) is an electrochemical method used in electrochemical analyzes by applying amplitude voltage pulses to a linear slope voltage. Where the latent value that does not occur in the Faraday change is chosen as shown in Figure 1.7, where the current is measured, and the difference is recorded before applying the pulse and at the end of the pulse as well [52].

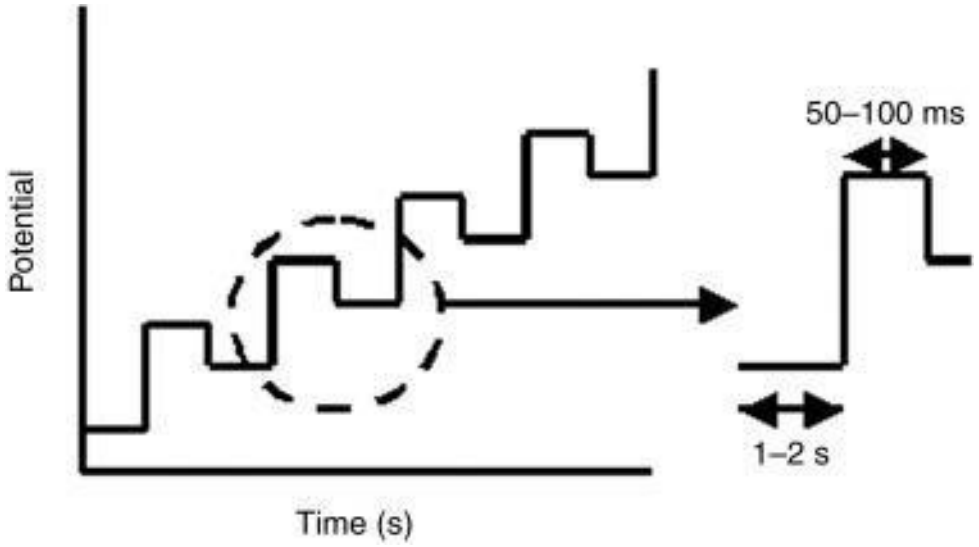

Figure 1.7 Diagram showing the application of pulses in a differential pulse voltammetry (DPV) technique [52].

1.15 Motivation

In this thesis, microelectrodes made of Au were integrated with Polydimethylsiloxane (PDMS) [53], made microchannels in different channel sizes, mainly the channel width, as shown in Figure 1.8, and their performance upon the integration were examined using CV, SWV and DPV. The effective microelectrode area was changed by changing the width of the microchannel. The ultimate purpose behind it is to produce different microelectrode areas with the microchannel integration, and to investigate the effect of microchannel integration on electrochemical response. The microchannel sizes varied from 500 µm to 250 µm, 100 µm and 50 µm.

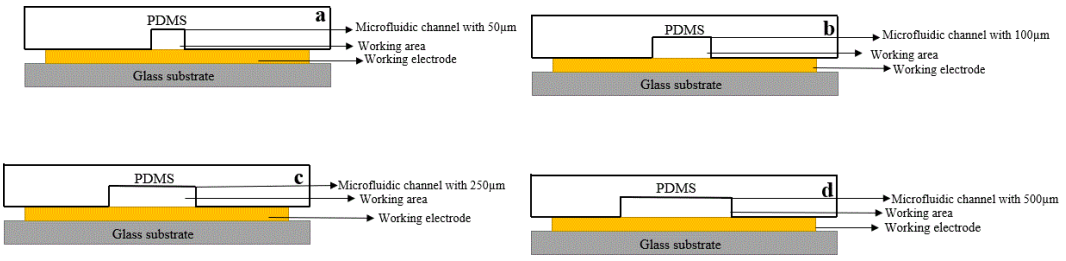

Figure 1.8 Schematic of device.

The concept of microelectrode integrated microfluidic channels is important because the potential use of the integrated technology in many label-free on-chip analytical

systems [54]. Microfluidic technology deals with fluids of small quantities through precise channels. Microfluidic technology general deals with fluids of small quantities through precise channels ranging from tens to hundreds of micrometers, as shown in Figure 1.9. This technology has shown its effectiveness in complex multi-domain laboratory [55]. Microfluidic devices are characterized by their small sizes, appropriate cost, and immense sensitivity for conducting numerous examinations to study of viruses, antibiotics, antibacterial, DNA amplification. This technology is also distinguished by its capability to process and integrate the automation of several cells, not one single cell.

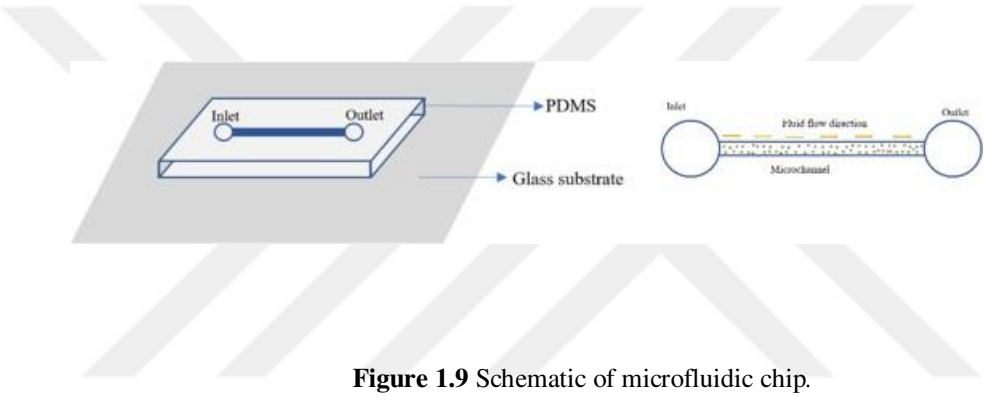

Figure 1.9 Schematic of microfluidic chip.

There are already reported microfluidic channel integrated microelectrode systems in the literature however, to do best of our knowledge, there is not any fundamental study on the relationship between microchannel size and effective microelectrode produced upon the integration. Therefore, we believe this study will provide fundamental information for future similar studies. For this purpose, our work was outlined as follows:

1. Design of microelectrode and microfluidic channels,

2. Production of microelectrode and microfluidic channels,

3. Integration of microelectrodes and microfluidic channels,

4. Characterization of channels by Dektak profilometer,

5. Characterization of microelectrodes by Atomic Force Microscopy (AFM) and Scanning Electron Microscopy (SEM)

6. Electrochemical measurements using CV, SWV, and DPV.

CHAPTER 2

EXPERIMENTAL PART

The experimental section includes the fabrication of microelectrodes, microfluidic channels, assembly, characterization, and electrochemical tests.

2.1 Fabrication of Microelectrodes

2.1.1 Design of Electrodes

Microelectrodes were designed using AutoCAD software by İremnur Akçakoca. First, a 26 mm X 26 mm glass slide was designed in the software and then microelectrodes were placed on top of the glass slide. As shown in Figure 2.1 showing the working electrode (WE) and reference/counter electrodes were installed on the glass substrate having dimensions of 1 mm and 0.2 mm respectively and with 4 mm contact pads.

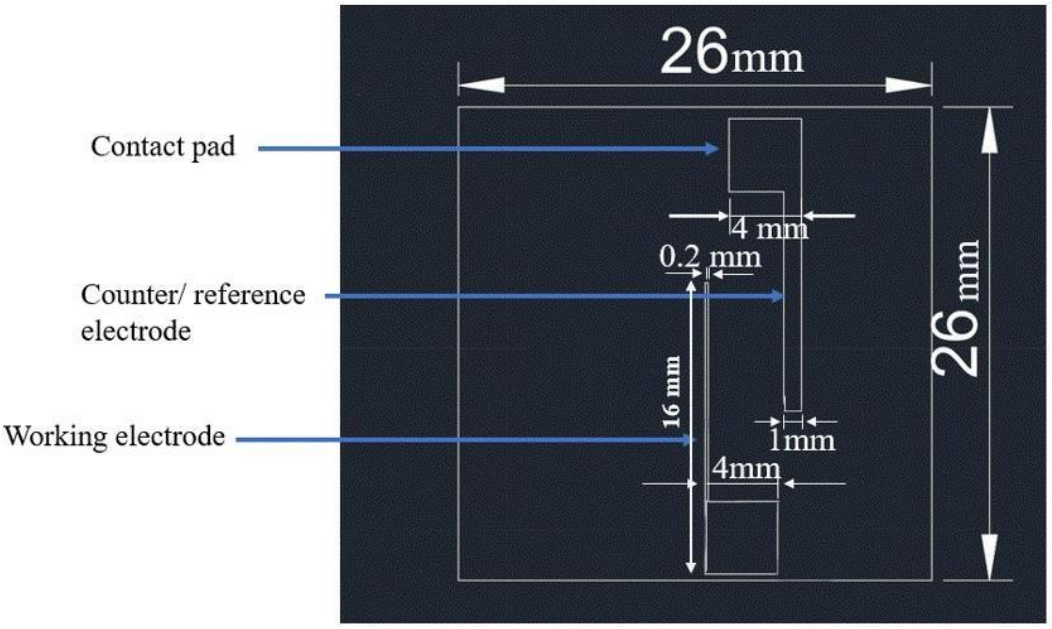

Figure 2.1 Design of gold microelectrodes.

2.1.2 Production of Microelectrodes

Shadow mask was produced by Photo Lab (Cambridge, UK) and the microelectrodes were fabricated by thermal evaporation as shown in Figure 2.2. Firstly, the glass slides were cleaned in an ultrasonic bath for 15 minutes with alcohol (isopropanol) and acetone then they were dried with nitrogen gas. 100 nm chromium (Cr) (99.99% Nanovak, Turkey) was deposited on the glass slide to enhance the adhesion of the gold layer to the glass substrate. After that, 300 nm gold (Au) (99.99%) (Nanovak, Turkey) was deposited on the adhesion layer. The thermal deposition process was carried out in Bilkent University, UNAM.

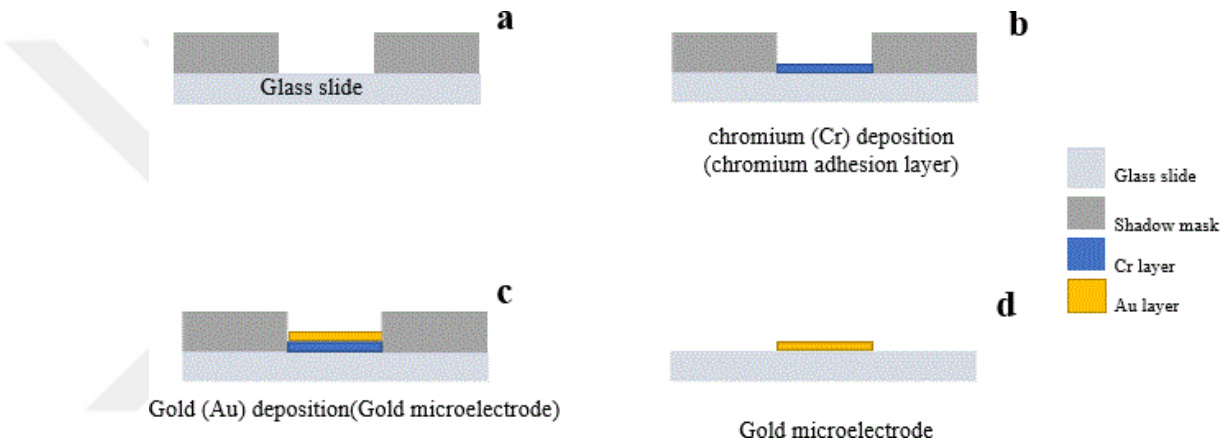

Figure 2.2 Schematic illustration for electrodes manufacturing process by thermal evaporation.

2.1.3 Characterization of Microelectrodes

Preliminary characterization of the device was carried out using an optical microscope (Euromex, Arnhem, The Netherlands.). Further characterization experiments were performed using AFM, SEM and Dektak Profiler measurments.

2.1.4 AFM characterization of Microelectrodes

Atomic Force Microscopy (AFM) (Quesant Q-Scope 250, Euromex, Nederlands) as shown in Figure 2.3 was used to characterize the microelectrode surface morphology. The microelectrode was cleaned, rinsed with deionized water for 10 seconds, dried with nitrogen, and then an AFM test was performed by applying following parameters (scan rate: 1 Hz, Scan angle: 0, Resolution: 512, Quesant Q Scope 250AND lateral

resolution: 1 nm). AFM scanning was performed by Dr. Abdullah Atılgan (Ankara Yıldırım Beyazıt University, Energy Systems Laboratory).

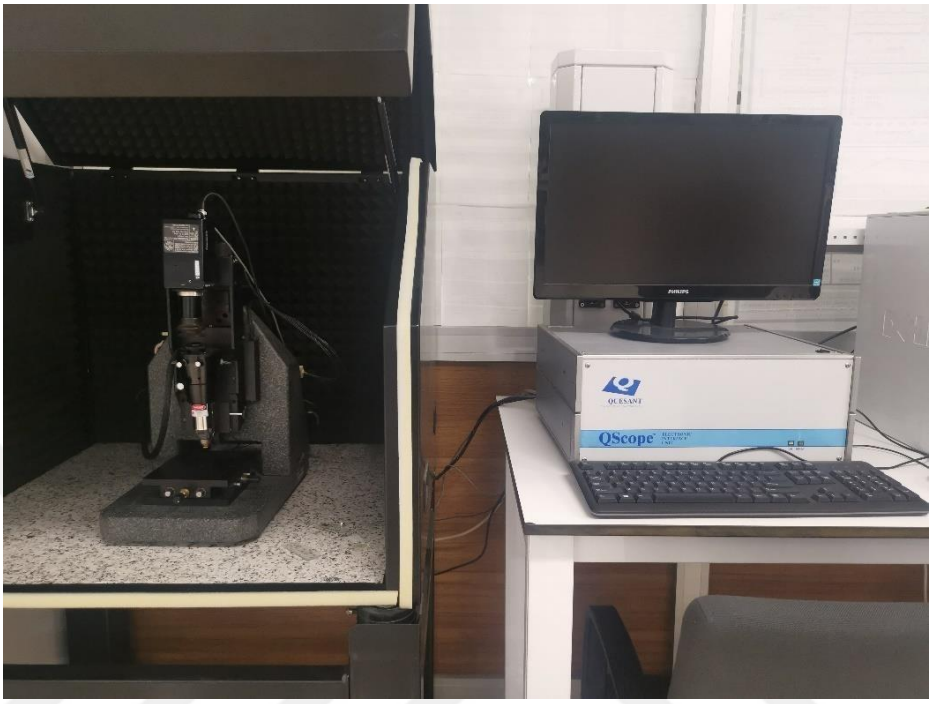

Figure2.3 Photograph image showing Atomic Force Microscopy (AFM).

2.1.5 SEM characterization of Microelectrodes

Scanning Electron Microscopy (SEM) examination was used in this experiment to investigate the microstructure and morphology of the surface of the gold microelectrodes. The test was carried out in the Central Laboratories of Ankara Yıldırım Beyazıt University by using (HITACHI SU5000 FIELD EMISSION SCANNING ELECTRON MICROSCOPE (FE-SEM)) as shown in Figure 2.5.
Following parameters was applied to carry out the SEM data Size=800x600, Pixel Size=13229.17, Working Distance=63519.59 um, Emission Current=125000 nA).

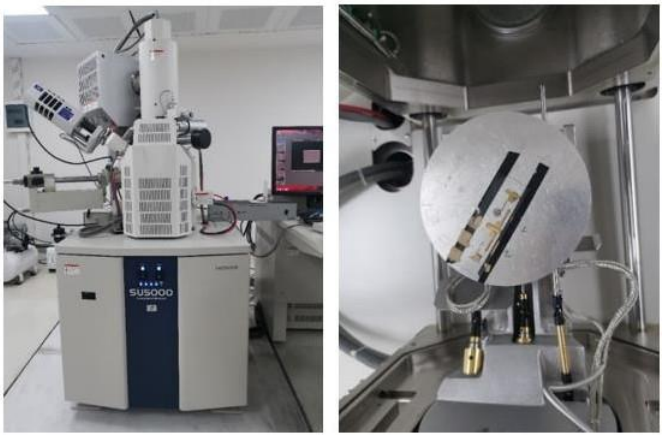

Figure 2.4 Photograph image showing Hitachi SU5000 Electronic Emission Scanning Microscope.

2.2 Fabrication of Microfluidic chip

2.2.1 Design of Microfluidic chips

The chip was designed by AutoCAD software by Dr. Hamed Ghorbanpoor and then transferred to the CORELDRAW software to fill the area of the photomask. The microchannels were made transparent, and the other parts were covered in black. Acetate photomask was produced by Cozum Tanitim, (Ankara), as shown in Figure 2.5.

Figure 2.5 Image of the 3-inch photomask design including all different chips with different microchannel widths.

2.2.2 Production of Microfluidic

Production was carried out using classical photolithography followed by soft lithography [53].

2.2.3 Production of Silicon template

Production of the silicon template was carried out using traditional optical photolithography method, as illustrated in Figure 2.6. The entire manufacturing process should take place in a clean room with a yellow light. Because the photoresist is a very sensitive process and reacts to ordinary light, the wavelength of light can avoid distortion in the process.

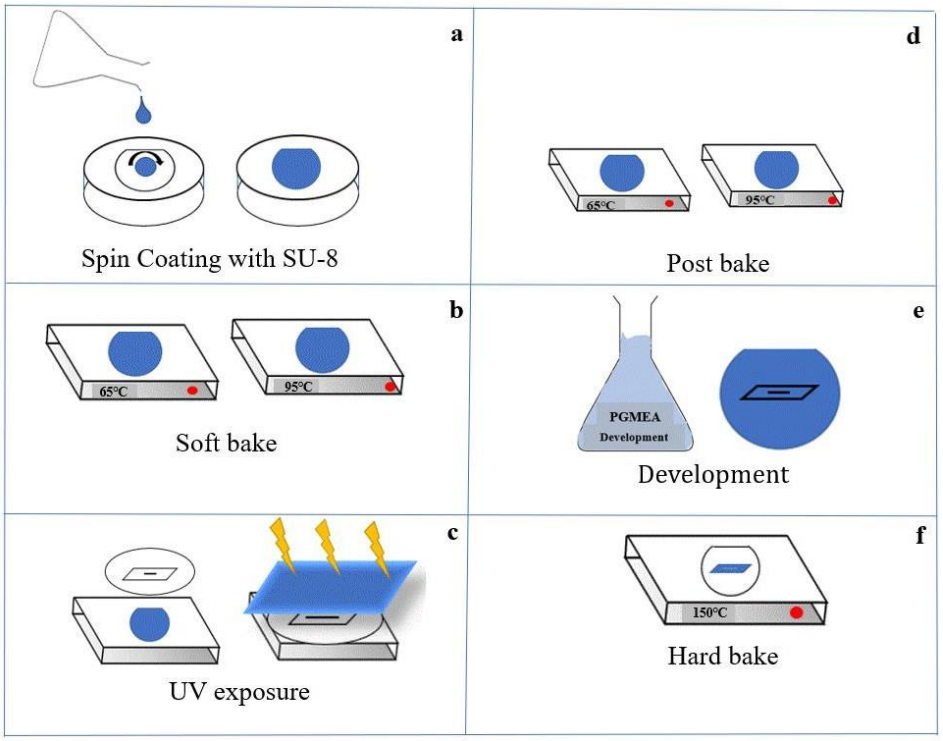

Figure 2.6 Flow diagram of silicon template fabrication.

After washing the silicon wafer with acetone, then with isopropyl alcohol, and lastly, rinsing with DI water and dried it with Nitrogen gas and putting it on the heater for 5 mins at 100 °C. 1 mL of photoresist SU-8 2050 was then applied on a 3-inch silicon wafer. The wafer was uniformly spin- coated with the photoresist by rotating it at 500

rpm for 15 seconds and then for 30 seconds at 3000 rpm (Laurell Technologies Corporation, USA). The wafer was then soft baked by leaving it on a hot plate (180 X180mm Plate-type Digital Precise Hotplate "MSH-20D" Package-set, Korea) for 3 minutes at 65 ºC and 7 minutes at 95°C, respectively as shown in Figure 2.7.

Figure 2.7 Photograph image showed setup of a) Spin coater and, b) Hot plate.

The mask was placed on the wafer coated with the photoresist, and to ensure that they touch together and prevent movement, adhesive tape was used around the mask and the wafers. The wafer was exposed to ultraviolet (UV) light with a wavelength of 265 nm for 225 seconds on the surface of the silicon wafer and the photomask as shown in Figure 2.8 Photolithography printing setting. a) Custom-made UV exposure system, and b) Setting for development process. After exposure to the light, the mask was carefully removed from the wafer and the wafer was placed for a minute on 65°C and 6 minutes on 95°C respectively for post-bake treatment. The development process of the wafer is carried out by pouring 50 ml of propylene glycol methyl ether acetate (PGMEA) was poured into the beaker Silicon wafer was put into PGMA and shaking for 5 minutes.

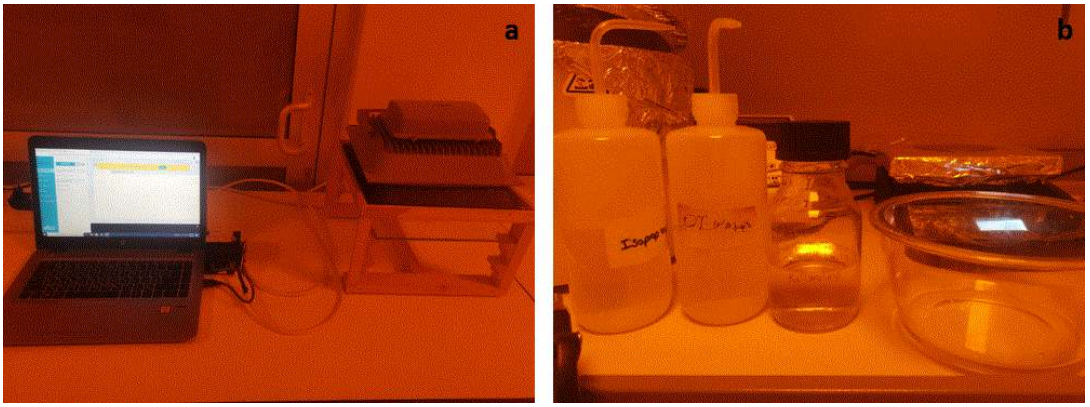

Figure 2.8 Photolithography printing setting. a) Custom-made UV exposure system, and b) Setting for development process.

Immediately after that, the wafer was washed with isopropanol and deionized water for 10 seconds. Then it was dried by nitrogen gas. For hard baking, the wafer was placed on a hot plate for 5 minutes at 150°C. Then the silicon template was produced as shown in Figure 2.9.

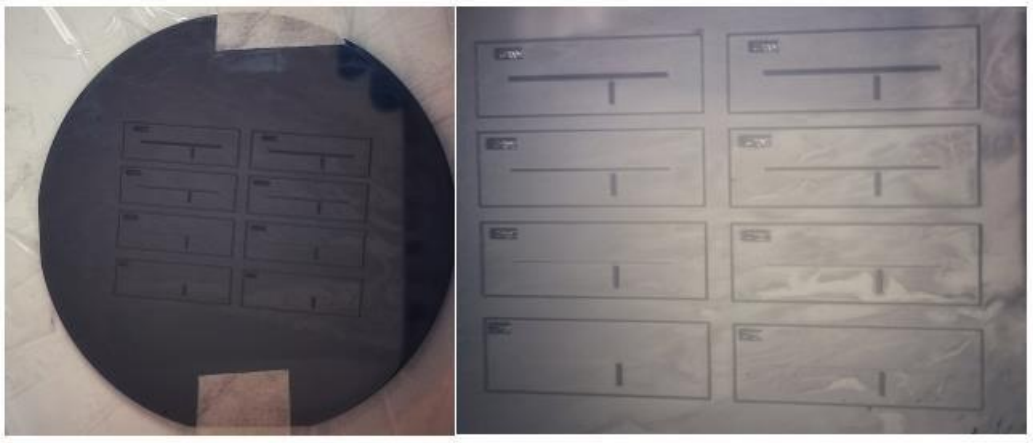

Figure 2.9 Fabricated silicon template.

2.2.4 PDMS casting

The microfluidic chips were produced using the soft lithography process using epoxy-based polydimethylsiloxane (PDMS). The PDMS kit (Sylgard 184, Dow Corning USA) contains two components: Primary elastomer and curing agent. Silicon template was placed in a petri dish as shown in Figure 2.10, then the PDMS basic elastomer

mixture and a well curing agent were added in a 10:1 ratio and the petri dish was left in a desiccator for 15 minutes to remove air bubbles.

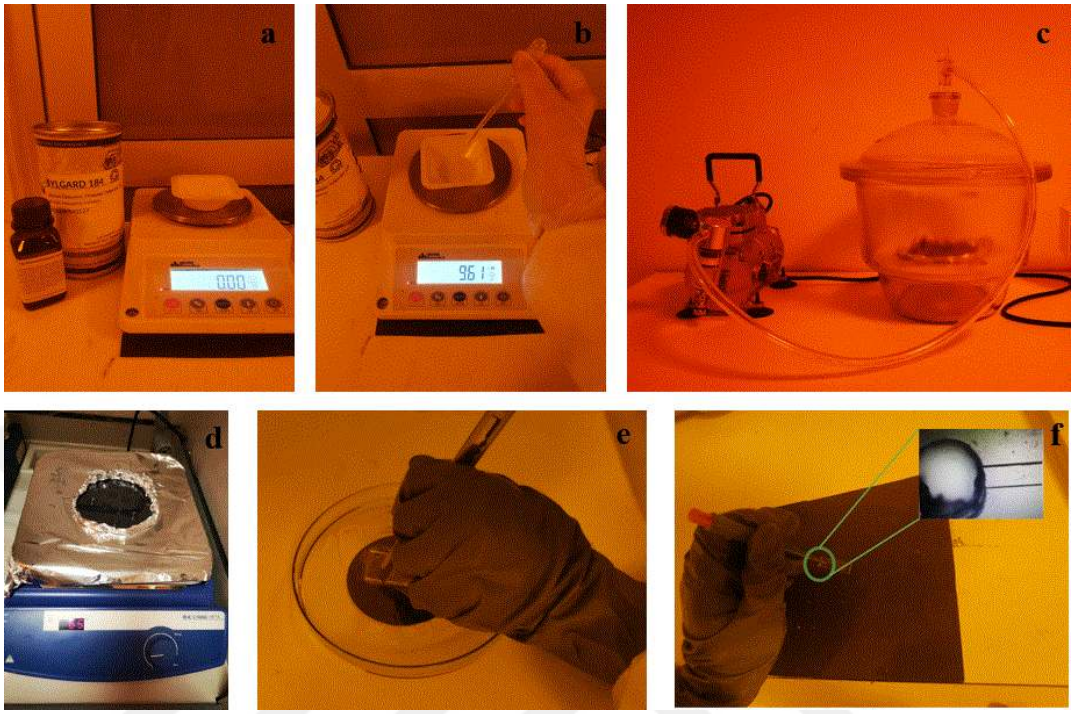

Figure 2.10 Steps to be followed to get the microfluidic chip.

Silicon template was left at 50 °C for 24 hours. After the time required for drying of the solution was completed, the individual microfluidic PDMS chips were carefully cut with a scalpel and peeled off from the template, with the designed patterns now transferred to the PDMS slap. Inlet and outlet holes were made in the channels with PDMS microfluidic chip biopsy puncture.

2.3 Assembly of Microelectrode integrated microfluidic chip

Assembly of the integrated chip was performed using a custom-made plasma device. Beforehand, the microelectrodes on glass and PDMS chips were first cleaned in 70% ethanol in an ultrasound bath for 5 minutes, then rinsed with deionized water and dried with nitrogen gas. The chips were then placed on the plasma device.

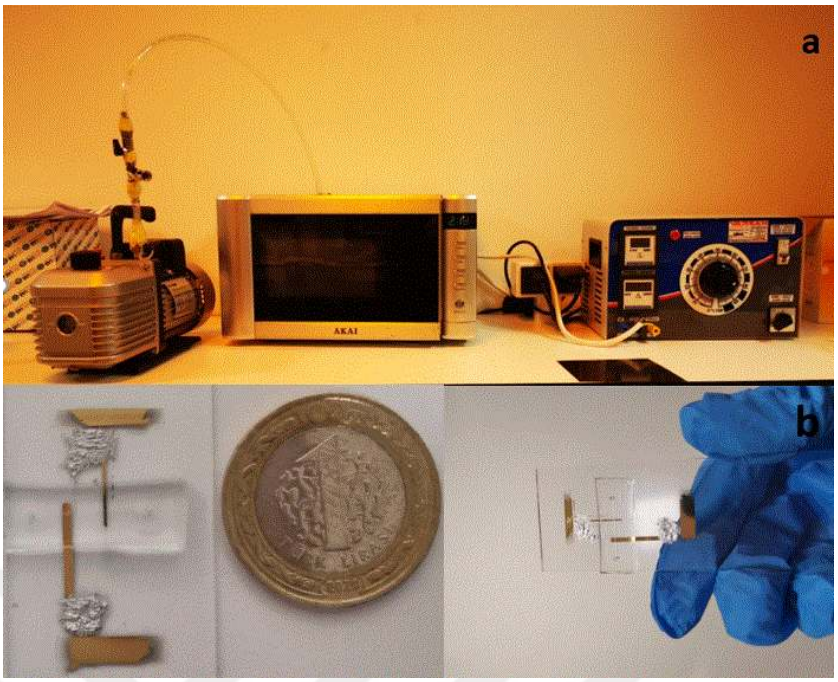

Figure 2.11 Bonding step: a) Photograph image showing the bonding system setup , b) Photograph image showing the size of chip.

The PDMS was chemically connected to the gold electrodes based on a glass slide through plasma exposure. The air plasma device is manually operated, after placing the PDMS slide and the glass slide a borosilicate glass cover was placed, after which the vacuum pump was operated. The microwave was turned on and, the plasma density is manually adjusted with the help of the varac device as shown in Figure 2.11. After 25 seconds, the microwave was turned off. Quickly take out the glass substrate, place it on a flat surface and place the PDMS chip directly on top of it, pressing it with hand to ensure enhanced adhesion. And we put it for two hours on the heater at 50 ° C, and to get a higher conductivity, as the last step, epoxy is added to the pads and left on the heater for 24 hours at 50 ° C and then the lab-on-chip is ready to work.

2.4 Electrochemical Experiments

In this experiment, the electrochemical measurements were characterized on and off the chip. Off-chip experiments were carried out with screen-printed gold electrodes (C220AT and C223AT). On-chip experiments were carried out with nonintegrated chip with hole PDMS and

integrated microfluidic chips with different channel widths (integrated chip 50 µm, integrated chip 100 µm, integrated chip 250 µm and, integrated chip 500 µm).

2.5 Off-chip electrochemical experiments

The screen-printed gold electrodes of 4 mm C220AT and 1.6 mm C223AT (SPEs) (Metrohm, Switzerland) as shown in Figure 2.12 was used for control experiments.

Figure 2.12 Off-chip experimental setup.

The electrodes were first rinsed with deionized water for 10 seconds, then dried and cleaned with a solution 0.1M H_2SO_4. A periodic CV was taken for each electrode by applying a voltage to both electrodes (C220AT and C223AT) ranging from -0.06 to 1.6 V until graph unchanging. After taking the CV using 0.1 M H_2SO_4 sulfuric acid, the electrodes were rinsed with deionized water, then 1 mM ferric/ferrocyanide solution, was added, and CV, SWV and, DPV measurements were performed.

2.6 On-chip electrochemical experiments

The electrodes were connected to the PalmSens4 via contact pads while the potentiostat was connected to a computer by a USB cable. To facilitate the connection of the gold electrodes to the PalmSense4 device, the integrated chips were fixed by a jig holder made of Plexiglas (PMMA) as shown in Figure 2.13. The jig was designed by Yasin Öztürk and produced by Yasin Öztürk and Vahit Güzel in (Pleksiart, Ankara, Turkey). The electrical connections were made by means of a micro-contact pad that is fixed by holes in the jig holder. The electrodes were first tested to ensure their safety

and ability to complete the experiment by placing a piece of BDMS containing a hole covering the area of each of the three electrodes. After making sure that the electrodes are safe, a specific protocol was applied to the electrodes in this experiment to conduct periodic cyclic voltammetry measurements. Pins were used to connecting the electrode to the Palm Sense device through a copper cable, one of its ends connected closely to the pins in contact with the electrode, and the other end is loose as it is connected to the Palm Sense cables.

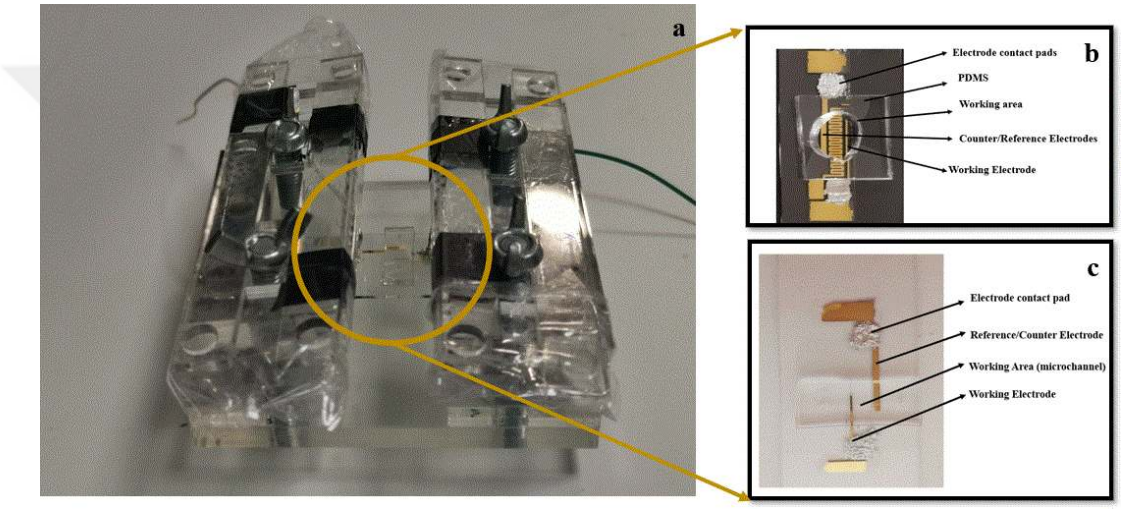

Figure 2.13 Image showing integrated chip setting, a) jig holder. b) Chip with BDMS, it has a hole to test the behavior of the electrodes before bonding them with the channels, c) Integrated microfluidic chip.

CHAPTER 3

RESULTS AND DISCUSSIONS

In this section, the classification of electrodes and channels in terms of size will be characterized, as well as the results of electrochemical measurements, and SEM and AFM characterization.

3.1 Design of Integrated chip

The microelectrode design included three electrodes: working electrode, reference electrode, and counter electrode. The dimensions related to the electrodes were as follows (the working electrode has a width of 0.2 mm and length of 16 mm, while the dimensions of the reference/counter electrode were 16 mm in length and 1mm in width) and the distance between the electrodes was chosen to be. Microchannels were selected with four different widths (50µm, 100µm, 250µm, and 500 µm). The effective electrode area of each electrode was calculated according to the channel size, as shown in Table 3-1 also shows the list of other samples used in the experiments: SPE with a WE of 1.6 mm , and 4mm in diameter, and non-integrated microelectrode sample used with a PDMS hole having an aperture to create the experimental chamber on it, the expected and obtained values were clarified.

Table 3-1 List of chips and dimensions chosen in the study.

Electrochemical characterization	No.	Expected					Experimental		
		Sample name	Diameter)mm)	Length (µm)	Width (µm)	Effective electrode area (mm^2)	Length (µm)	Width (µm)	Effective electrode area (mm^2)
OFF	1	SPE 1.6	1.6	-	-	-	-	-	-
	2	SPE 4	4	-	-	-	-	-	-
ON	1	Non-integrated chip							
	2	Integrated chip 50 µm	-	200	50	0.01	362	49	0.01
	3	Integrated chip 100 µm	-	200	100	0.02	347	158	0.05
	4	Integrated chip 250 µm	-	200	250	0.05	364	254	0.09
	5	Integrated chip 500 µm	-	200	500	0.1	396	463	0.1

Microfluidic chip has a single channel design with different width dimensions were chosen as mentioned in the above table respectively, upon the integration. Optical images of each integrated chip are shown in Figure 3.1.

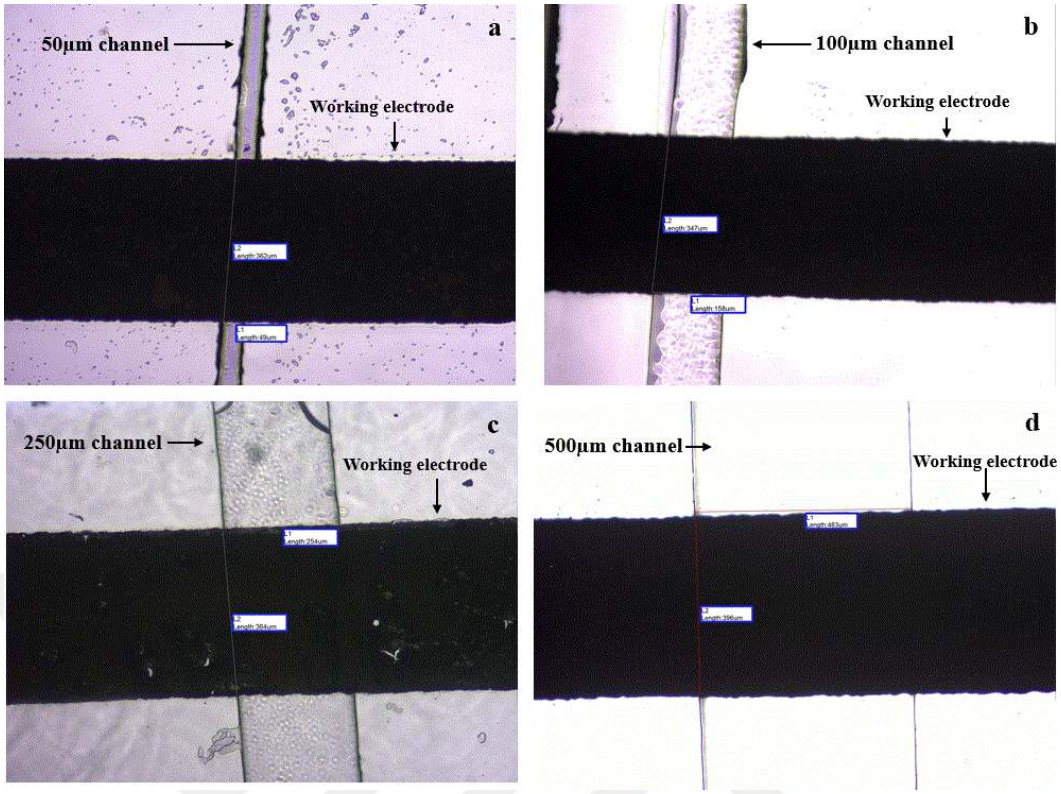

Figure 3.1 Optical image for integrated microfluidic chips. a) Sample integrated chip 50 µm, b) Sample integrated chip 100 µm, c) Sample integrated chip 250 µm and, d) Sample integrated chip 500 µm.

Due to the challenges encountered during the photolithography process to produce microfluidic films (disclosure will be presented in the next section), the expected dimensions cannot be obtained and the reason for the fabrication process such as wavelength, UV exposure time, or development process other protocol variants. These results mentioned above are the ones that were finally obtained.

3.2 Characterization of Microchannels

To obtain the certified chip with accurate or close values, some parameters (UV time, heating time, and development time) were changed several times as mentioned in Table 3-2.

Table 3-2 Lithography parameters chosen for the optimization of the production. Resulted thickness values were measured from 3 different parts of the same wafer and averaged.

Experiment	1.spin	2.spin	Soft Bake	UV Exp. Time sec	Post Bake	Development min	Comments
1	15sec/500rpm	30sec/3000 rpm	3min at 56°C 6min at 95 °C	180	1min at 56°C 7min at 95°C	2:30	50 µm channel width was not obtained.
2	15sec/500rpm	30sec/3000 rpm	3min at 65°C 7min at 95°C	180	1min at 65°C 6min at 95°C	5	50 µm channel was printed but it was not valid for experiments.
3	15sec/500rpm	30sec/3000 rpm	3min at 65°C 7min at 95°C	190	1min at 65°C 6min at 95°C	3	All channels were produced, and they were of dimensions close to the expected dimensions.
4	15sec/500rpm	30sec/3000 rpm	3min at 65°C 7min at 95°C	195	1min at 65°C 6min at 95°C	2:30	The dimensions of the obtained channels were smaller than the expected dimensions.
5	15sec/500rpm	30sec/3000 rpm	3min at 65°C 7min at 95°C	204	1min at 65°C 6min at 95°C	5	The obtained dimensions of some channels were too far from the expected dimensions.
6	15sec/500rpm	30sec/3000 rpm	3min at 65°C 7min at 95°C	225	1min at 65°C 6min at 95°C	3:30	The dimensions of the obtained channels were larger than the expected dimensions by about 30 µm.

After conducting several experiments, Experiment No. 3 was obtained with a measurement appropriate to complete the experiment. A-side was adopted to produce the micro-channels as shown in Figure 3.2.

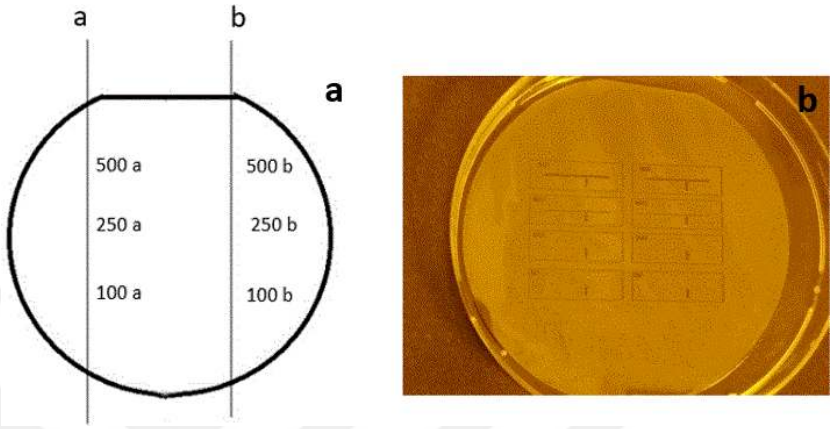

Figure 3.2 Certified silicone template. a) Schema of a 3-inch silicon wafer, b) Photography image of the 3-inch silicon wafer.

The Produced microchannels were subjected to Dektak profilometer measurements to cognize the accurate width of the channels compared to the assumed width, and the results were as mentioned in Table 3-3:

Table 3-3 A table showing the expected values of the microchannels and the obtained values after the manufacturing process.

Expected Channel size	Experimental Channel size
500 µm	463 µm
250 µm	254 µm
100µm	158 µm
50µm	49 µm

3.3 Characterization of Microchannels using Profilometer measurements

Dektak provides the ability to quickly and easily set up and run automated multi-location measurement procedures to determine the exact thickness of thin films on a wafer surface with unparalleled repeatability. The Dektak self-aligning pen and assembly allows users to change the size of the pen tip while eliminating any mishaps quickly and easily during the process. The implementation of a mono-arch structure makes the Dektak more robust, reducing the source of environmental noise. Dektak's "smart electronics" uses a state-of-the-art processor that minimizes temperature changes and reduces error-causing noise, resulting in a more powerful system capable of measuring heights below 10nm for full operation and analysis [56]. The examination is carried out by moving the diamond pen perpendicular to the surface of the sample and upon contact with the surface as shown in Figure 3.3, it is moved horizontally across the sample for a specified distance and contact force. The profilometer can measure small differences in the surface. A typical profilometer can measure small vertical features that range in height from 10 nanometers to 1 millimeter. The position of the height of the diamond pen generates an analog signal that is converted into a digital signal, stored, analyzed, and displayed. The radius of the diamond pen ranges from 20nm to 50μm, and the horizontal resolution is controlled by the scanning speed and data signal sampling rate. The pen's tracking strength can range from as little as 1 to 50 milligrams [57].

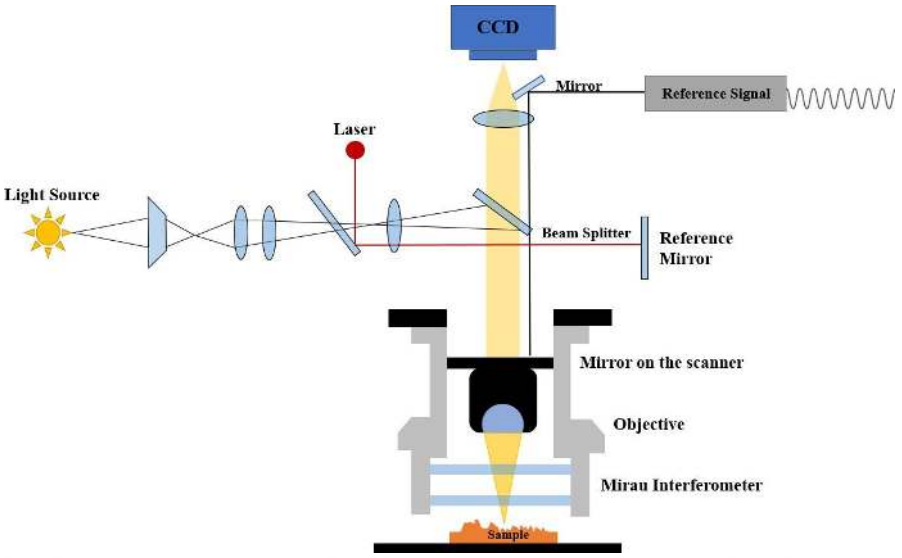

Figure 3.3 Diagram of the optical profilometer measurement.

Channels were characterized by profilometer measurement, the results were analyzed by Microsoft Origin Pro2021program, the results of the analysis were as shown in Figure 3.4.

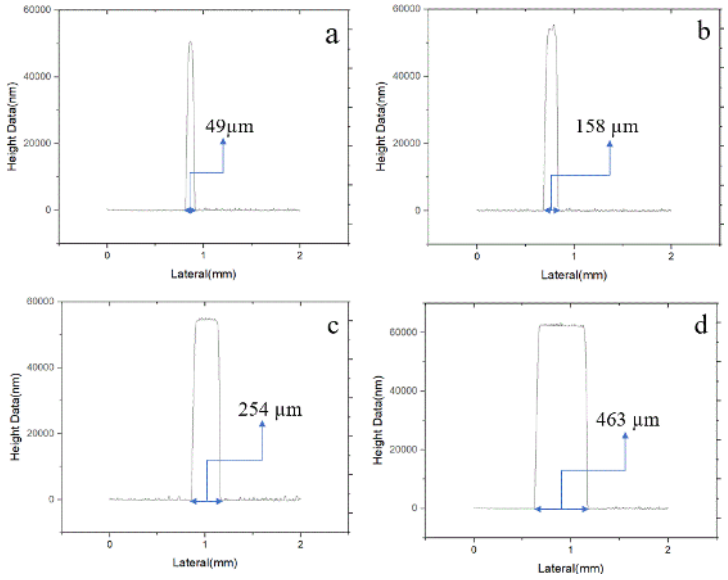

Figure 3.4 Profilometry results of microfluidic channels. a) Chip 50 µm, b) Chip 100 µm, c) Chip 250 µm and, d) Chip 500 µm.

3.4 Characterization of Microelectrode

Characterization of the microelectrodes were performed using Atomic Force Microscopy (AFM) and Scanning Electron Microscopy (SEM) to find out the morphological surface properties of the electrodes produced after the thermal evaporations.

3.4.1 Characterization of Microelectrodes using Atomic Force Microscopy (AFM)

It is a device that uses an atomic energy to know the topography of surfaces with nano- and even micron dimensions. In recent years, the use of this device has diversified, as it has become used in other measurements, such as measuring the flexibility of nano and micron particles and cells. It is also used to measure the adhesion energy between chemical molecules, nano and micron particles, and cells. The device consists of a needle with micron dimensions that passes over the surface to be scanned, this needle is fixed to a horizontal holder while it is itself perpendicular to this holder and on the surface to be scanned, a laser beam is dropped on the holder, which rises and falls with the rise and fall of the needle and thus With the variety of surface topography from high and low, the laser beam is captured on the holder on a receiver and thus the topography of the scanned surface is determined and drawn according to the movement of the laser beam reflection as shown in Figure 3.5 [58]. One disadvantage of AFM compared to SEM is the image size. The SEM device can measure an area of a few millimeters and a depth of a few millimeters, but the AFM device works on an area of 150 X 150 µm and a depth of 10-20 µm. But this shortcoming was addressed by the development of AFM devices by IBM that works with two parallel sensors. Also, using an improper probe tip may give some defects in the resulting image. In addition to the fact that AFM operates slowly compared to SEM that gives a live image of the sample, the AFM requires that it work for a few minutes until it gives an image. This delay results in a thermal shift in the image, which makes the atomic force microscope unsuitable for accurate measurements of topographical distances on the image. To overcome this problem, AFM devices are being developed with devices known as video AFM that operate faster than SEM [59].

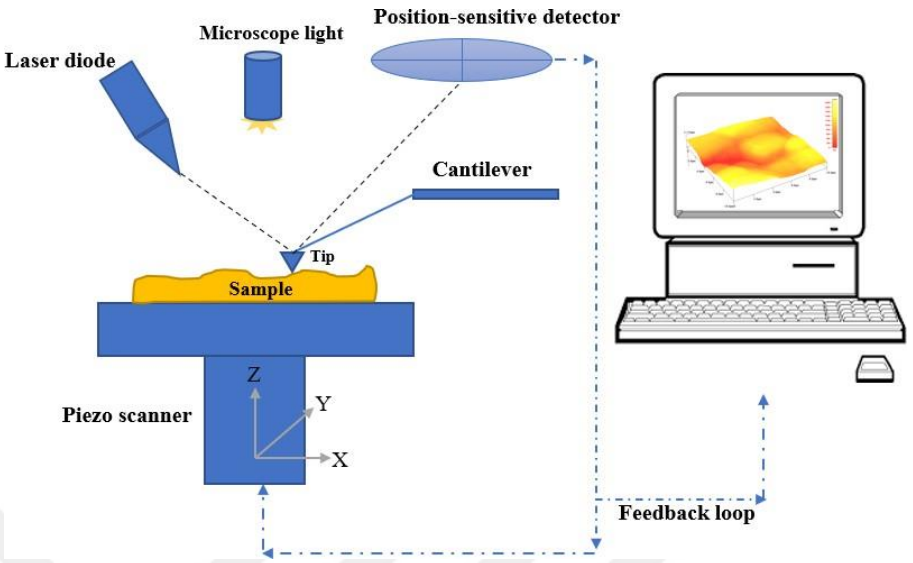

Figure 3.5 Schematic showing the working principle of the atomic force microscope (AFM).

When comparing the microscopic images of the screen-printed gold electrode and the gold microelectrodes manufactured by thermal evaporation as shown in Figure 3.6 . It was noticed that the surface roughness of the printed electrode was much less than the surface roughness of the integrated microfluidic chip and that the surface tends to be smooth, which leads to better performance, while there is an inverse relationship between the surface roughness and the accuracy of the results. As the accuracy of the results in the experiments also depends on the surface roughness, as the adhesion of the particles of the solutions to be examined is greater if the surface is less rough.

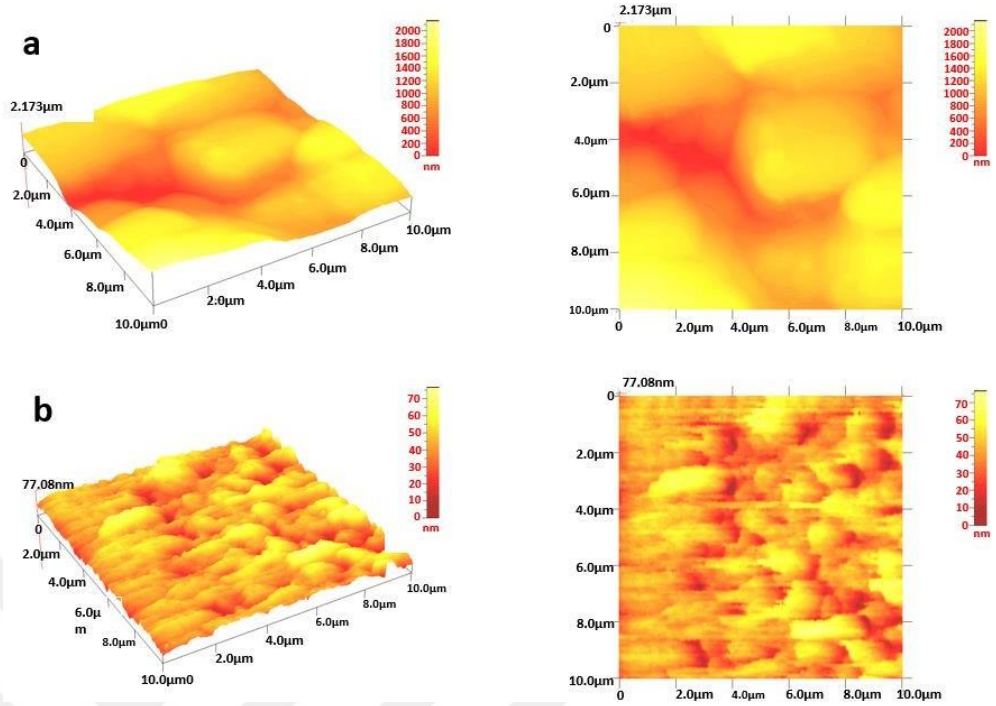

Figure 3.6 AFM image. a) Screen printed gold electrode, b) Microfluidic chip.

3.4.2 Characterization of Microelectrodes using Scanning electron microscopy (SEM)

The scanning electron microscope can be characterized by a quite high magnification power of more than half a million times, and the reason for this is due to the use of electron radiation, which is a high-energy electron beam with a very short wavelength in the range of 0.0068 nm, so we find that the resolution of this resolution The microscope reaches less than 0.5 nm and the power of discrimination means the ability of the microscope to distinguish "distinguishing" between two closely spaced objects so that they appear separate, and this depends on the wavelength used, which makes it very strong discrimination. The theory of the work of the scanning electron microscope depends on the use of a high-energy electronic beam that hits the surface of the sample vertically and then collects the reflected signals from the sample using different detectors as shown in Figure 3.7. In the following we will provide a simplified explanation of how this microscope works:

1. The electrons are produced by heat emission by means of a heating filament usually made of tungsten, and an acceleration voltage is applied to this filament whose value varies from 0.1 V to 30 V.
2. The electron beam passes through the vacuum microscope column, and this beam is focused by a group of electromagnetic lenses along this column.
3. The apertures located along with the microscope column control the width of the electron beam by trapping the scattered electrons and Deviated packet path. The electronic beam collides with the surface of the sample, which is inside a closed and completely vacated space called the scanning electron microscope room (SEM chamber), where this beam interacts with the sample surface, and this interaction results in several emissions “signals”. Each signal is collected by its own detector, then these signals were be analyzed and processed, then shown as images [60].

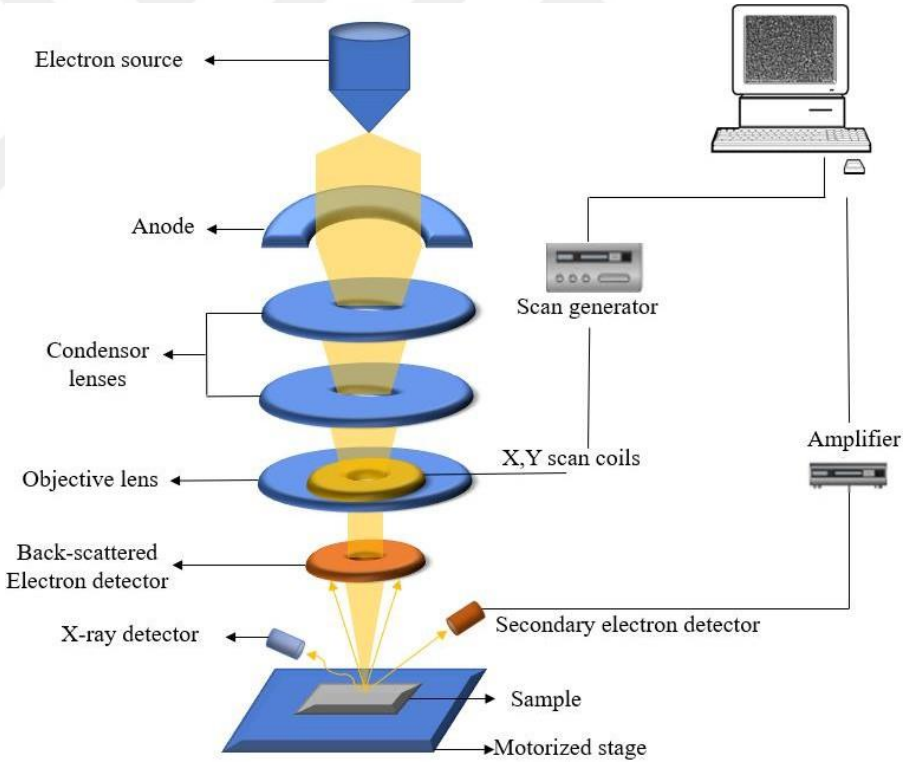

Figure 3.7 Schematic showing the working principle of the Scanning electron microscopy (SEM).

SEM was used to demonstrate their surface properties and molecular structure.

Figure 3.8 shows the SEM images of C220AT and integrated microfluidic chip. The microscopic images of hybrid-chip show the metal particles of different sizes and how they affect sensitivity as the size of the grains is an important characteristic where the greater the decrease in the grain size, the stronger the metal becomes because the distance at which disturbances occur be shorter. The ratio of surface area to volume was greater when the size of grains was smaller, which means that the ratio of grain boundaries to turbulence increases, and the greater the grain boundaries, the greater the strength. As for the printed electrodes, a heterogeneous surface with accumulated sheets aligned with each other was observed, which increases the surface roughness and the intensity of its change.

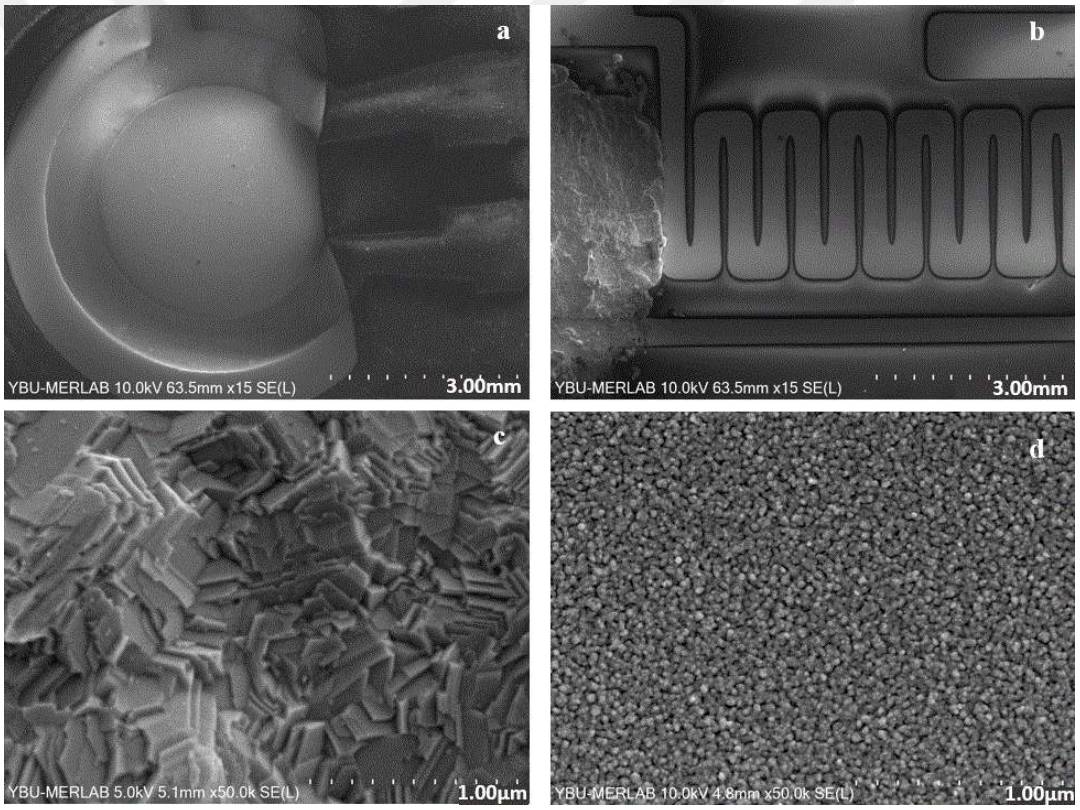

Figure 3.8 SEM image: a) Screen printed gold electrode C220AT ,b) Microfluidic chip, c) Microstructure of SPE surface and d) Microstructure of microfluidic chip surface.

3.5 Electrochemical Characterization

The process of cleaning the electrodes was recorded with H_2SO_4 from between 0.0V to 1.6V until the stability of the oxidation and reduction peaks were unchanged. The electrodes are characterized by cyclic voltammetry (CV) at 1 mM ferric/ferrocyanide between -0.6 V to +0.6 V. The measurements of SWV and DPV were taken at the same range of voltage.

3.5.1 Cleaning of Electrodes

The characterization of the macro and micro gold electrodes by the cleaning procedure was carried out and voltage cycling in 0.1 M H_2SO_4 and the Cyclic Voltammetry (CV) of the integrated microfluidic chip from 0.0V to 1.6V in scan rate 100 mV until the graph unchanged as shown in Figure 3.9.

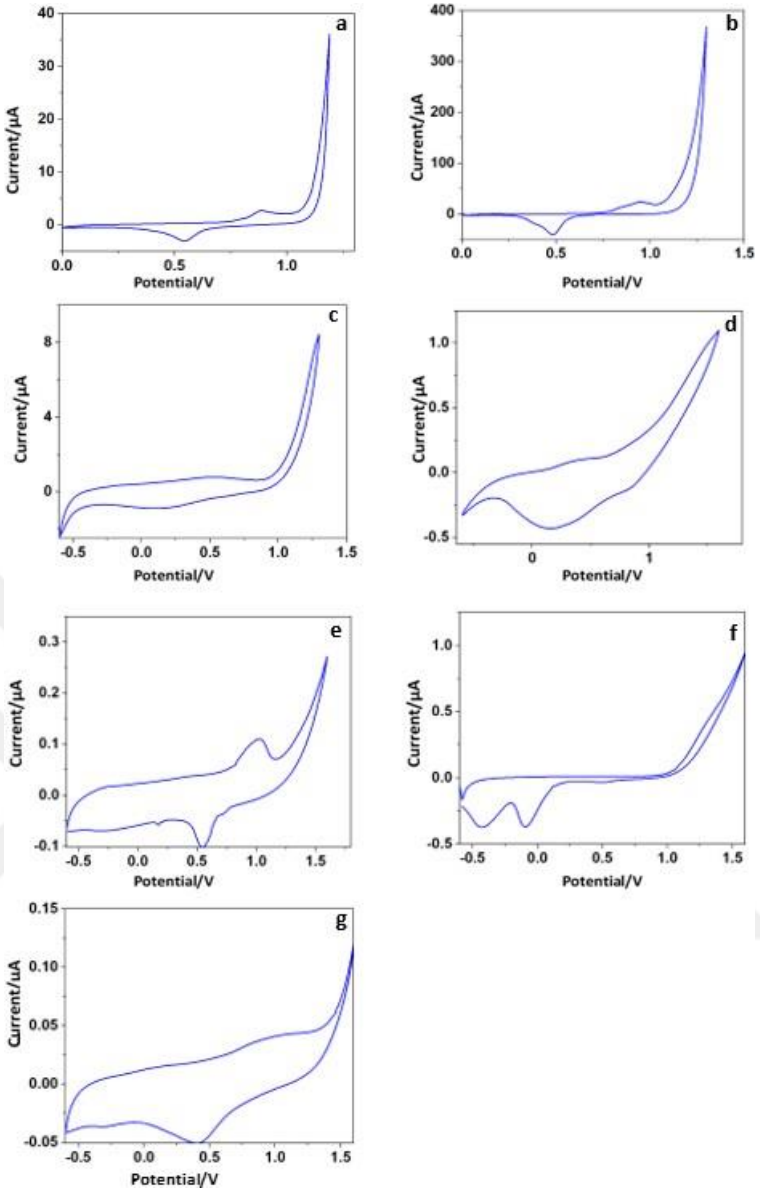

Figure 3.9 CV of microelectrodes in 0.1 M H_2SO_4. a) SPE C223AT, b) SPE C220AT, c) Nonintegrated chip, d) Chip 50 µm, e) Chip100 µm, f) Chip 250µm, and g) Chip 500 µm.

3.5.2 Characterization of Electrodes using redox molecules

The cleaning quality was characterized by measuring CVs in 1 mM Ferric/ferrocyanide solution which is a redox couple. CV was cycled between -0.6 V and +0.6 V until the graph was unchanged, and Figure 3.10 shows the CV of SPEs and integrated microfluidic chip. Peaks separations were analyzed to characterize the electrode cleaning performance. The separation values of 100 mV were calculated for each

sample and the results were in line with the expected value obtained according to the Nernst equation. This then proves that the cleaning process was successful.

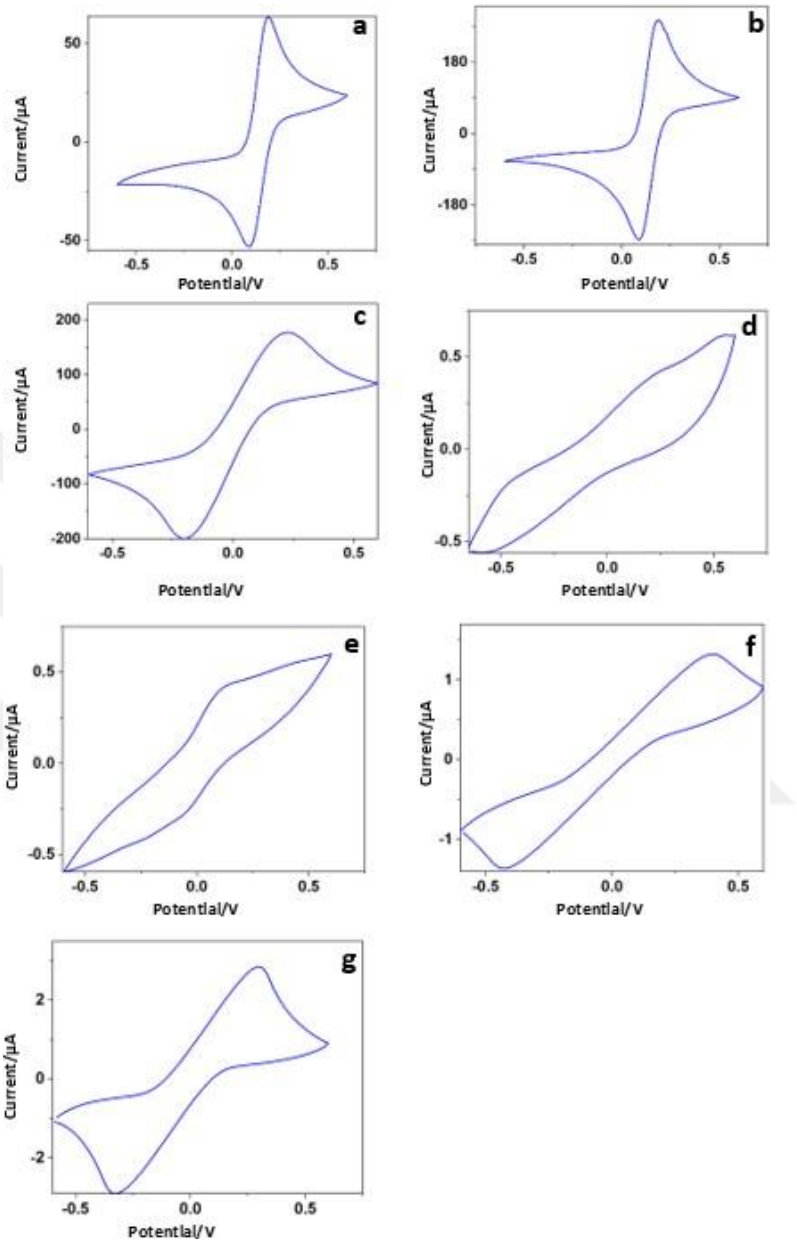

Figure 3.10 CV of microelectrodes in in 1 mM FF. a) SPE C223AT, b) SPE C220AT, c)Nonintegrated chip, d) Chip 50 µm, e) Chip100 µm, f) Chip 250µm, and g) Chip 500 µm.

As a result, ((CV) were compared) for work areas of different sizes. It was found that all the hybrid slices of channels with a width (50µm, 100µm, 250µm, and 500µm) behave as a microelectrode. We can deduce this from the cyclic voltammetry (CV)

measurement results which are shown in Figure 3.11. The figure shows us the captive expectations for the unique difference between the electrodes, although all electrodes behave as a micro-convergent diffusion is a type which is evident in this experiment, the CV shape changes from one area to another due to the change in the diffusion rate.

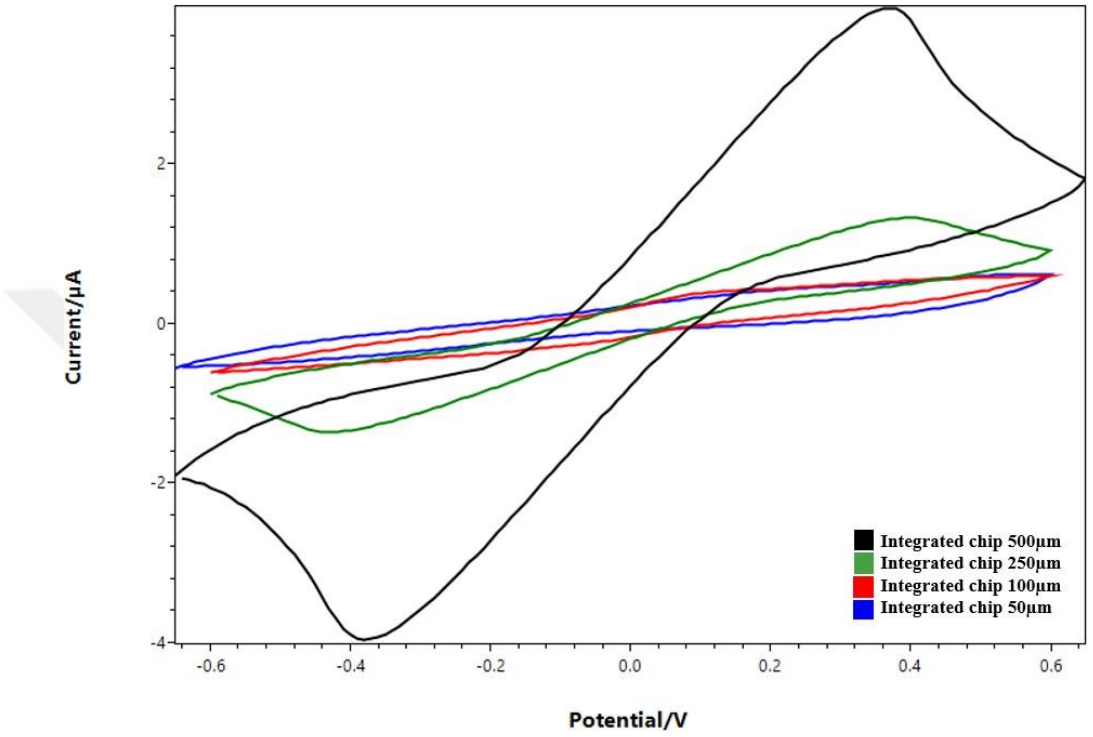

Figure 3.11 Cyclic voltammetry (CV) for integrated chips.

Electrode characterization was performed using SWV as shown in Figure 3.12 for screen printed gold electrode (C223AT and C220AT) and the integrated electrodes of different working area sizes to describe the gradual modification of polarity in 1M Ferric/ferrocyanide solution. High, sharp, and clear peaks are observed for some electrodes, due to the increase in the working region, which leads to an increase in the electron transfer rate, while low peaks mean a decrease in the peak current, due to the delay in the arrival of the redox molecules to the surface, due to the small area.

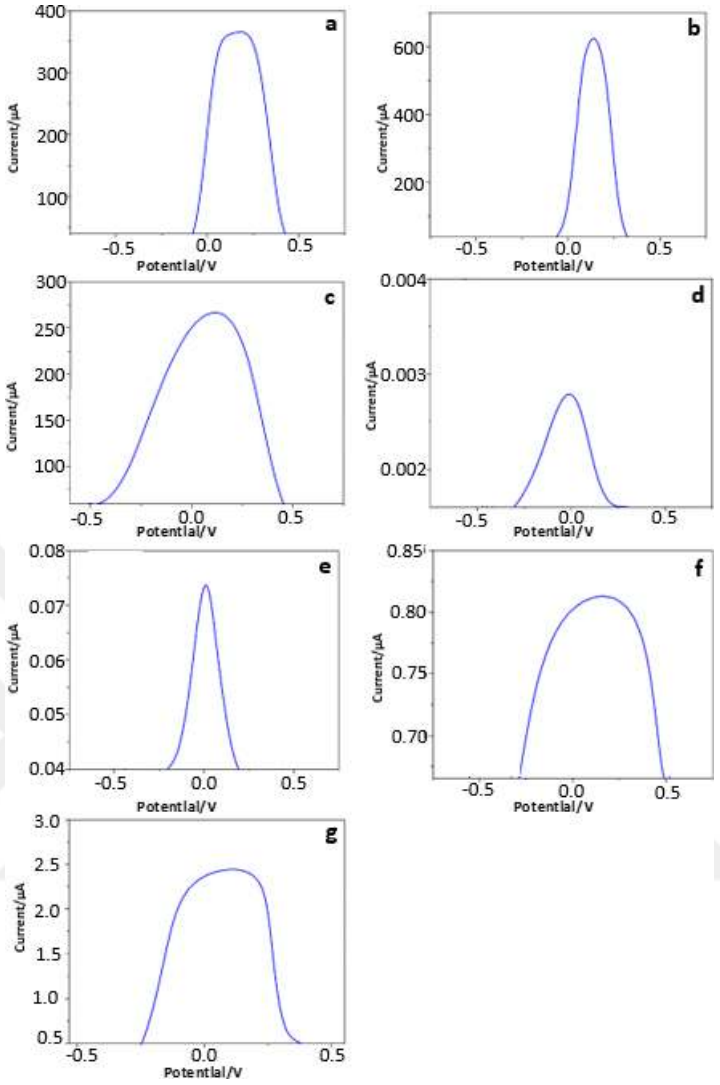

Figure 3.12 SWV of microelectrodes in 1 mM a) SPE C223AT, b) SPE C220AT, c)Nonintegrated chip, d) Chip 50 µm, e) Chip100 µm, f) Chip 250µm, and g) Chip 500 µm.

The results of the differential pulse voltammetry (DPV) were taken for screen printed gold electrode(C223AT and C220AT) and the integrated electrodes of different working area sizes as shown in Figure 3.13. The method of measuring differential pulse voltammetry (DPV) technique is more accurate than measuring cyclic voltammetry (CV)and in presenting the results because of its increased sensitivity and its ability to detect concentrations much lower than the concentrations detected by cyclic voltammetry (CV). Concentrations were detected by the cyclic voltmeter (CV).

Through the results, it was noted that the concentrations of peaks are low at the small area of the working electrodes and increase with the increase in the working area of the electrode.

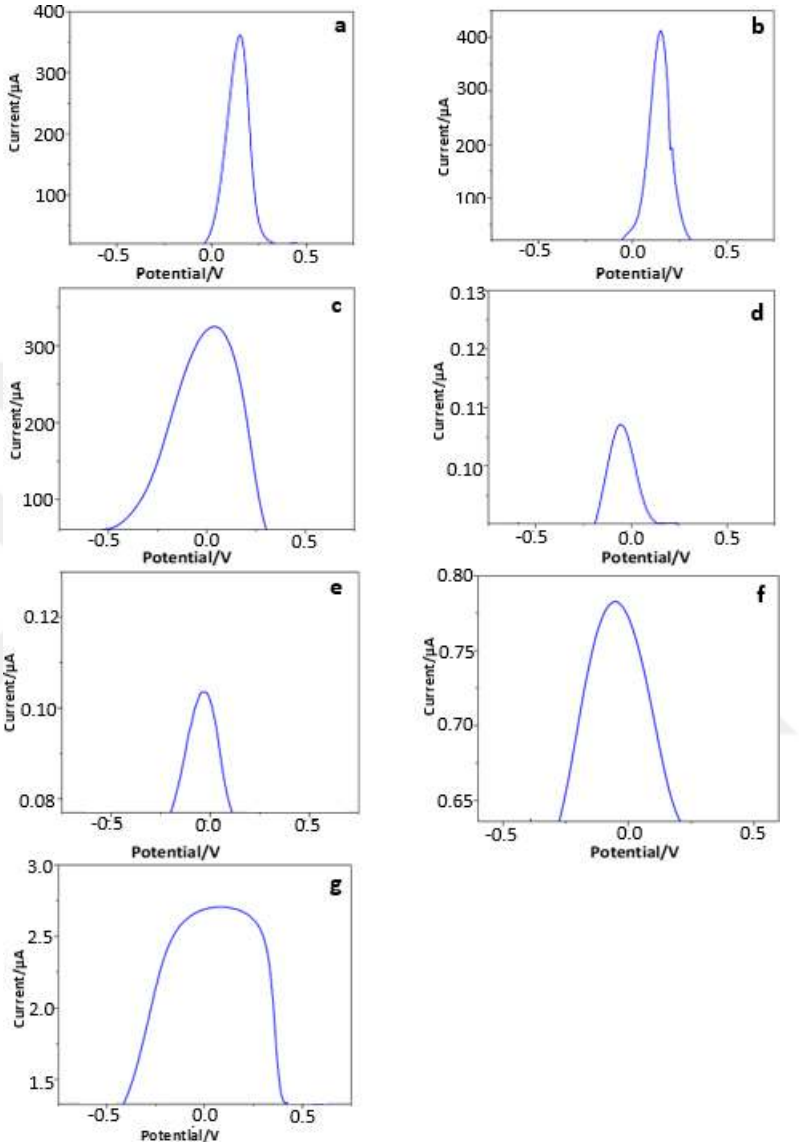

Figure 3.13 DPV of microelectrodes in 1 mM FF a) SPE C223AT, b) SPE C220AT, c)Nonintegrated chip, d) Chip 50 µm, e) Chip100 µm, f) Chip 250µm, and g) Chip 500 µm.

3.6 Effect of Scan rate

Scan rate plays an important role in cyclic voltammetry measurements. Scanning the potentials in the forward and reverse directions provides us with an opportunity to

know the type of chemical behavior of the electrodes, which makes the cyclic voltammetry measurement distinct from the rest of other voltammetry Analysis Methods. Figure 3.14 shows us the cyclic voltammetry (CV) diagram for the same microelectrode with the same potential range -0.6V to +0.6V, but with different scanning rates, faster and slower. We notice from the figure that the faster the scanning rate, the clearer the oxidation and reduction peaks. Since the fast-scanning rate results in a larger concentration inclination near the electrode, which results in higher current and increases the speed of electron transfer and thus a balance occurs between the oxidation and reduction peaks. Randle's–Ševčík equation for liquids at 25 °C was applied to a chip 250 µm and chip 500 µm microfluidic channel integrated onto microelectrode, where the area of the active region of the electrode was 0.09 and 0.5 mm^2 respectively with changing the scan rate. The results for Integrated chip 250 µm and 500 µm are shown in Figure 3.. Unfortunately, we were not able to obtain results from Chip 50 µmand 100 µm. For Integrated chip 250 we were only able to obtain results from three different scan rates (0.05, 0.04 and 0.03 v/s) and for chip 500 two different scan rates were applied (0.06 and 0.04 v/s).

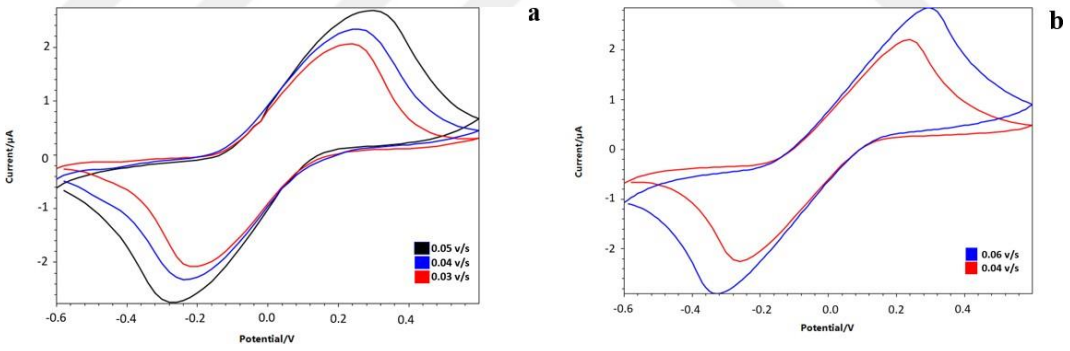

Figure 3.14 Cyclic voltammogram of microelectrode with different scan rate.

In Table 3-4 the results of the expected current and the current values obtained during the experiment were recorded for each scan rate.

Table 3-4 Table showing the obtained and theoretical current values for different scan rates for the same effective area of the electrode.

Sample name	No.	Scan rate (V/s)	Theoretical current (µA)	Experimental current(µA)
250	1	0.05	1.824	2.457
	2	0.04	1.631	2.055
	3	0.03	1.413	2.006
500	1	0.06	3.294	2.845
	2	0.04	2.690	2.381

In conclusion, Table 3-5 provides a summary of the electrochemical findings for off-chip and on-chip experiments. In terms of explaining the CV graphs and giving a brief description of the shape of the oxidation-reduction peaks resulting from the SWV measurement and describing the shape of the peaks of the concentrations obtained from the DPV measurement.

Table 3-5 Table provides a summary of the electrochemical findings for off and on chip experiments.

	Off chip experiment			On chip experiment
	C220AT	C223AT	Off-chip microelectrode	Microelectrodes integrated microfluidic chip
CV	By recording the shape of the CV and the emergence of the peaks, it was observed that the working pole behaves as a macroelectrode	By recording the shape of the CV and the emergence of the peaks, it was observed that the working pole behaves as a macroelectrode	By recording the shape of the CV and the emergence of the peaks, it was observed that the working pole behaves as a macroelectrode	By recording the shape of the CV and the emergence of the peaks, it was observed that the working pole behaves as a macroelectrode
SWV	The oxidation and reduction peaks were clear and prominent due to the large area of the work area	The oxidation-reduction peaks were less visible and prominent due to the small area of the work area	The oxidation-reduction peaks were less visible and prominent due to the small area of the work area	The oxidation and reduction peaks ranged in clarity and prominence due to the difference in the effective area of the working electrode, which was clearer when the area increased
DPV	The concentrations of peaks are high due to the large size of the working electrode	Concentration of peaks are lower due to the small size of the working electrode	The concentrations of peaks are low due to the small effective area of the working electrode	The concentrations of peaks range from being low to high due to the difference in the active region of the working electrode

CHAPTER 4

CONCLUSION AND FUTURE DIRECTIONS

4.1 Conclusion

In this study, the behavior of the integrated working electrode on the microfluidic chip was studied by changing the effective area of the electrode by changing the width of the microfluidic channels. Channels with widths closer to the expected width were produced by experimenting with several protocols. Accordingly, electrochemical experiments were carried out off-chip and on-chip and compared with each other.

CV, SWV, and DPV examinations were conducted for four different working areas, in which the electrode acted as a macroelectrode, this was observed by observing the behavior of the electrode through the shape of the resulting CV and changing the oxidation and reduction peaks. The results showed that the larger the effective area, the better the electrode performance and peaks became clearer, due to the increase in electron transfers.

The scan rate was also changed, the theoretical current values were compared with the values obtained during the experiment, it was also noted that the higher the scanning rate, the more visible the oxidation and reduction peaks, due to allowing the entry of larger amounts of current. The microscopic structure of the electrode was also studied by conducting an SEM examination. The microscopic structure of the electrodes consisted of small grains that give the surface strength. And by conducting an AFM examination to study the surface roughness, it became clear from this that the electrode has a roughness ratio, which may affect the mechanism of adhesion of the atoms of the solutions to be examined, and thus affect the sensitivity.

4.2 Future Directions

The integrated chips can be used in biological and electrochemical experiments, and it is possible to try other deposition methods for gold electrodes to obtain a better surface finish. Also, smaller channel dimensions should be investigated to examine the

threshold which determines the cross-over point from macroelectrode behavior to microelectrode.

REFERENCES

[1] Tallman, D.E.(2011). Microelectrodes for voltammetry—a personal historical perspective Solid State Electrochemistry 15.

[2] Delahay, P. (1954). New instrumental methods in electrochemistry. New York.

[3] Nicholson, R. S., & Shain, I. (1964). Theory of stationary electrode polarography. Single scan and cyclic methods applied to reversible, irreversible, and kinetic systems Analytical chemistry, 36(4), 706-723

[4] Jean, M ,S.,& Cyrille,C. (2006). Elements of molecular and biomolecular electrochemistry. Willey-VCH, New Jersey.

[5] Allen, J. B.,& Royce, W. M. (2012, July ,17). Electrochemistry,), 11484-11486. Proceedings of the National Academy of Sciences.

[6] Wilhelm, O. (1980). Electrochemistry, history and theory: Electrothermies: Ihre Geschichte und Lehre. New Delhi. Smithsonian Institution and the National Science Foundation.

[7] Michael, S.,& Jonathan,P.M.(2018). Microelectrode Recording in Functional Neurosurgery.Researchgate,177187.https://www.researchgate.net/publication/326399743_Microelectrode_Recording_in_Functional_Neurosurgery.

[8] Richard, C. A., Dieter, M. K., Jacek, L., Phil, N. R. (2009). Chemically modified electrodes (Vol. 22). John Wiley & Sons.

[9] Harper, A., & Anderson, M. R. (2010). Electrochemical Glucose Sensors—Developments Using Electrostatic Assembly and Carbon Nanotubes for Biosensor Construction. *Sensors,10*(9), 8248-8274. doi:10.3390/s100908248.

[10] Allen., & Larry,R.F. (2001). Fundamentals and applications Electrochemical Methods, 2(482), 580-632.

[11] Ronald, J. M.(1993). Theoretical Mechanics of Biological Neural Networks .321-336 Chapter 20 - Contextual Overview of Organization in Cortical Networks

[12] Dorothee, G., Robert, M., Janos, V., & Erik,R.(2008). Electrochemical biosensors-sensor principles and architectures. Sensors, 8(3), 1400-1458.

[13] Takurou, N.M.,⁻Norimichi, K., & Tsutomu, M. (2005). A high-voltage dye-sensitized photocapacitor of a three-electrode system. Chemical communications, (26), 3346-3348.

[14] Larry, B. A., & Charles, N. R.(1965). Thin-layer electrochemistry: use of twin working electrodes for the study of chemical kinetics. Journal of Electroanalytical Chemistry (1959), 10(5-6), 538-552.

[15] Bertrand ,D., Daniel, G., Robert, D., & Duncan. W. B. (2003). Comprehensive coordination chemistry II. J. Mc Cleverty, TJ Meyer, Eds, 761-773 1.44.

[16] Peter,T.K; &William R. (1996-01-23). Laboratory Techniques in Electroanalytical Chemistry,Revised and Expanded (2ED.).Routledge. https://www.routledge.com/Laboratory-Techniques-in-Electroanalytical-Chemistry-Revised-and-Expanded/Kissinger

[17] Joseph, W., Baomin, T, & Eskil, S.(1999). Integrated electrophoresis chips/amperometric detection with sputtered gold working electrodes. Analytical Chemistry, 71(17), 3901-3904.

[18] David, J .I.,& George, J. J.(1961) .2. The Hydrogen Electrode. Reference Electrodes. New York . https://www.worldcat.org/title/reference-electrodes-theory-and-practice/oclc/543041

[19] William, E. G. (2007). Organometallic Electrochemistry: Origins, Development, and Future. Organometallics. 26 (24): 5738–5765. https://pubs.acs.org/doi/abs/10.1021/om700558k

[20] Allen, J.B., Larry, R. F. (2000). Electrochemical Methods: Fundamentals and Applications (2 ed.). Wiley

[21] Honeychurch, K. C. (2012). Printed thick-film biosensors. Printed films, 366-409.

[22] Stuart, F. C. (2008). Neural stimulation and recording electrodes. Annu. Rev. Biomed. Eng., 10, 275-309.

[23] Engineering Materials Science 1995, Pages 559-610 Engineering Materials Science 11 - ELECTRICAL PROPERTIES OF METALS, INSULATORS, AND DIELECTRICS.

[24] Walter, T. H. (2014). Electrochemical Characterization of Mass Transport at Microelectrode Arrays. Revista de Ciencias, 18(1), 101-110.

[25] Santhisagar,V.,Ioannis,T.,Diane,J.B.,Faquir,C.J.,&Fotios,P. (2010). Emerging synergy between nanotechnology and implantable biosensors: a review. Biosensors and Bioelectronics,25, 1553-1565.

[26] Francois, G.C.& Richard ,G. C. . (2006). Regular arrays of microdisk electrodes: numerical simulation as an optimizing tool to maximize the current response and minimize the electrode area used. Electroanalysis: An International Journal Devoted to Fundamental and Practical Aspects of Electroanalysis, 18, 2369-2374.

[27] Gusphyl, J., Abdur, R.A. R., & Anthony, G.2009. Bioactive hydrogel layers on microdisk electrode arrays: cyclic voltammetry experiments and simulations. Electroanalysis: An International Journal Devoted to Fundamental and Practical Aspects of Electroanalysis, 21, 1125-1134.

[28] Richard ,L. M., (2008). Advanced carbon electrode materials for molecular electrochemistry. Chemical reviews, 108(7), 2646-2687.

[29] Petr ,Z.(2000). Role of mercury electrodes in contemporary analytical chemistry. Electroanalysis: An International Journal Devoted to Fundamental and Practical Aspects of Electroanalysis, 12(15), 1187-1194.

[30] Allen, J. B.,Larry, R. F., LR (2001) Electrochemical methods. Fundamentals and applications. Wiley, New York, NY.

[31] Salvatore, D.,& Carlo ,B. (2014). From macroelectrodes to microelectrodes: Theory and electrode properties. In Environmental analysis by electrochemical sensors and biosensors (pp. 373-401). Springer, New York, NY.

[32] Walker, Jearl; Halliday, David; Resnick, Robert (2014). Fundamentals of physics (10th ed.). Hoboken, NJ: Wiley. p. 749. ISBN 9781118230732. OCLC 950235056.

[33] Salvatore, D.,&Carlo, B. 2014. From macroelectrodes to microelectrodes: Theory and electrode properties. Springer, New York, NY.

[34] Ian, M.F.,Harindra, V.,& Alexander ,S.2010. Biosensors based on one-dimensional nanostructures. Journal of Materials Chemistry.10, 1377-1398

[35] Hayder, A.A,& Esmail, A. M.B.2017. Electrochemical biosensors: electrode development, materials, design, and fabrication. ChemBioEng Reviews, 4, 92-105.

[36] Comprehensive Chemical Kinetics Volume 26, 1986, Pages 79-143 Chapter 2 Mass Transport to Electrodes Author links open overlay panel Keith B.Oldham Cynthia G.Zoski.

[37] Benjamin, R.S., (1988). Diffusion to ensembles of microelectrodes. Journal of electroanalytical chemistry and interfacial electrochemistry, 240(1-2), 61-76.

[38] Kelly, R. S. (2009). Analytical electrochemistry: the basic concepts. Analytical Sciences Digital Library.

[39] Joseph ,W. (2001). Analytical Electrochemistry. New York.

[40] Antonio,D.,Leandro,M.D.,Mariele,M.,Drochss, P.V.,& Gerardo,C., . (2015). Electrochemical monitoring of the pharmacological activity of natural products. In Studies in Natural Products Chemistry (Vol. 45, pp. 59-84). Elsevier. Chapter

3 - Electrochemical Monitoring of the Pharmacological Activity of Natural Products.

[41] Sanjun, Z.,Lotfi, B.,Juan, E.,Thibault ,R.,Cendrine ,F.M.,&Françoise, A.(2007). Surface plasmon resonance characterization of thermally evaporated thin gold films. Surface Science, 601(23), 5445-5458.

[42] Hongyan, C., Xiaobo, X., Shengpu, X., Leanne, L. H. C.,& Yong ,H.(2019).Electrochemical characteristics of microelectrode designed for electrical stimulation. Biomedical engineering online, 18(1), 1-14.

[43] Mohaddeseh, V., Manouchehr, V., Raheleh, M., & Pezhman, S. (2019). Gold-plated electrode with high scratch strength for electrophysiological recordings. Scientific reports, 9(1), 1-11.

[44] Keith,S.,& Eileen, H. Y. (2015). Microbial electrochemical and fuel cells: fundamentals and applications. Woodhead Publishing.

[45] Cyclic Voltammetry. (2020, August 16). Retrieved May 23, 2021, from https://chem.libretexts.org/@go/page/311.

[46] Bansod, B., Kumar, T., Thakur, R., Rana, S., & Singh, I. (2017). A review on various electrochemical techniques for heavy metal ions detection with different sensing platforms. Biosensors and Bioelectronics, 94, 443-455.

[47] Noémie, E., Kelley, J. R., Brian, D. M., Eric, S. R., Thomas ,T. E.,& Jillian ,L. D. (2018). A practical beginner's guide to cyclic voltammetry. Journal of chemical education, 95(2), 197-206.

[48] Xudong, X. (2005). Assessment of an ultramicroelectrode array (UMEA) sensor for the determination of trace concentrations of heavy metals in water. Univ.-Verlag Karlsruhe.

[49] Piero ,Z., Carlo,N.,& Fabrizia, F.D. . (2019). Inorganic electrochemistry: theory, practice and application. Royal Society of Chemistry.

[50] John, T. S. (1993). A backward look at scientific instrumentation. Analytical Chemistry, 65(7), 344A-351A

[51] Allen, J. B.&Larry, R. F. (2001). Fundamentals and applications. Electrochemical Methods, 2(482), 580-632.

[52] Siti, N. H. U., Elmi, A.B.,Noorfazreena ,M. K., & Naoki ,U. (2020). A Prototype Development and Evaluation of Electrochemical Device for Heavy Metal Measurement. In Proceedings of International Conference of Aerospace and Mechanical Engineering 2019 (pp. 117-125). Springer, Singapore.

[53] Mihrimah, O.,& Michael, H.(2007). BioMEMS and biomedical nanotechnology: volume II: micro/nano technologies for genomics and proteomics (Vol. 2). Springer Science & Business Media.

[54] Markus, F., & Andreas, N.(2006). PDMS microfluidic chip with integrated waveguides for optical detection. Microelectronic Engineering, 83(4-9), 1291-1293.

[55] Eve, M., Benoit. C., Aurélie, G., Frédéric, S ., & Maxime, C. (2018). An integrated microfluidic/microelectrode array for the study of activity-dependent intracellular dynamics in neuronal networks. Lab on a Chip, 18(22), 3425-3435.

[56] Aaron, M. S., & Yanyi, H. (2013). Chip in a lab: Microfluidics for next generation life science research. Biomicrofluidics, 7(1), 011302.

[57] Younan, X., & George, M. W. (1998). Soft lithography. Annual review of materials science, 28(1), 153-184.

[58] Hoo, C. M., Starostin, N., West, P., & Mecartney, M. L. (2008). A comparison of atomic force microscopy (AFM) and dynamic light scattering (DLS) methods to characterize nanoparticle size distributions. Journal of Nanoparticle Research, 10(1), 89-96.

[59] Eduardo,L.,Joaquín,G.&Ángela,M. (2014). Recent advances on the theory of pulse techniques: A mini review. Electrochemistry communications, 43, 25-30.

[60] McMullan, D. (1995). Scanning electron microscopy 1928–1965. Scanning, 17(3), 175-185.

[61] Nicholson, R. S., & Shain, I. (1964). Theory of stationary electrode polarography. Single scan and cyclic methods applied to reversible, irreversible, and kinetic systems Analytical chemistry, 36(4), 706-723.

[62] Jean, M ,S.,& Cyrille,C. (2006). Elements of molecular and biomolecular electrochemistry. Willey-VCH, New Jersey.

September 2021
ANKARA

Department of Material Engineering

Zahraa Ali